Ein hochstabiler Laser als optisches Frequenznormal

DIPLOMARBEIT

zur Erlangung des akademischen Grades

Diplom-Ingenieur

im Rahmen des Studiums

Technische Physik

eingereicht von

Thomas Tobias Pronebner, BSc
Matrikelnummer 01129159

an der Fakultät für Physik

der Technischen Universität Wien

Betreuung: Univ.Prof. Dipl.-Phys. Dr.rer.nat. Thorsten Schumm
Mitwirkung: Dr. Michael Matus
Dr. Jörg Premper

Wien, 11. Juli 2021

Thomas Tobias Pronebner | Thorsten Schumm

An ultra-stable Laser as an optical frequency standard

DIPLOMA THESIS

submitted in partial fulfillment of the requirements for the degree of

Diplom-Ingenieur

in

Technical Physics

by

Thomas Tobias Pronebner, BSc
Registration Number 01129159

to the Faculty of Physics

at the TU Wien

Advisor: Univ.Prof. Dipl.-Phys. Dr.rer.nat. Thorsten Schumm
Assistance: Dr. Michael Matus
Dr. Jörg Premper

Vienna, 11th July, 2021

Thomas Tobias Pronebner | Thorsten Schumm

Technische Universität Wien
A-1040 Wien ▪ Karlsplatz 13 ▪ Tel. +43-1-58801-0 ▪ www.tuwien.ac.at

Erklärung zur Verfassung der Arbeit

Thomas Tobias Pronebner, BSc

Hiermit erkläre ich, dass ich diese Arbeit selbständig verfasst habe, dass ich die verwendeten Quellen und Hilfsmittel vollständig angegeben habe und dass ich die Stellen der Arbeit – einschließlich Tabellen, Karten und Abbildungen –, die anderen Werken oder dem Internet im Wortlaut oder dem Sinn nach entnommen sind, auf jeden Fall unter Angabe der Quelle als Entlehnung kenntlich gemacht habe.

Wien, 11. Juli 2021

Thomas Tobias Pronebner

Danksagung

An erster Stelle möchte ich mich bei meinen Eltern bedanken, die mir ein sorgenfreies Studium ermöglicht haben und mir jederzeit mit Rat und Tat zur Seite gestanden sind.

Des Weiteren möchte ich Thorsten Schumm für die angenehme Betreuung und die unheimlich nette Umgangsart danken. Trotz vollen Terminkalenders fand sich immer rasch ein Termin um meine Fragen oder Sorgen zu klären.

Ein besonderer Dank gebührt dem BEV und meinen Kollegen im BEV, die mich nicht nur in fachlicher Hinsicht stets hilfsbereit beraten haben. Ich durfte von Michael Matus, Anton Nießner und Werner Mache sehr viel Wissen aufnehmen und die direkte Zusammenarbeit mit den Kollegen Georg Zechner, Jörg Premper und Elke Aeikens hat viel zu dieser Arbeit beigetragen. Auch möchte ich Christina Hofstätter-Mohler und Petra Milota danken, die mir die Stelle im BEV ermöglicht haben.

Da diese Arbeit im Rahmen des EMPIR Projektes CC4C entstanden ist, hatte ich die Gelegenheit internationale Partner kennenzulernen. Den Kollegen des ISI in Brünn Ondrej Cip, Martin Cizek, Lenka Pravdova, Pham Minh Tuan und Jan Hrabina bin ich sehr dankbar, dass sie mir mit viel Geduld und Freundlichkeit ihr Wissen weiter gegeben haben.

Acknowledgements

First of all, I would like to thank my parents, who made it possible for me to study carefree and who were always on hand with advice and assistance.

Furthermore, I would like to thank Thorsten Schumm for being my supervisor and the incredibly friendly manner. Despite his busy schedule, an appointment was always quickly found to clarify my questions or concerns.

A special thank you goes to the BEV and my colleagues at BEV, who always gave me helpful advice, and not just in technical matters. I was able to gain a lot of knowledge from Michael Matus, Anton Nießner and Werner Mache. The direct collaboration with colleagues Georg Zechner, Jörg Premper and Elke Aeikens has contributed a lot to this work. I would also like to thank Christina Hofstätter-Mohler and Petra Milota, who made it possible for me to work at BEV.

Since this thesis was written within the framework of the EMPIR project CC4C, I had the opportunity to get to know international partners. I am very grateful to the colleagues at the ISI in Brno, Ondrej Cip, Martin Cizek, Lenka Pravdova, Pham Minh Tuan and Jan Hrabina, for sharing their knowledge with me with great patience and kindness.

Kurzfassung

Nach mehr als einem halben Jahrhundert als primäres Frequenznormal sind Cäsium-Atomuhren an die Grenzen der Weiterentwicklung der Präzision gestoßen und eine Ablösung durch einen präziseres Normal zeichnet sich ab. Die potentiellen Nachfolgernormale sind sogenannte optische Uhren, deren Taktgeber eine elektromagnetische Welle im optischen Teil des Frequenzspektrums ist. Diese optischen Uhren erreichen deutlich höhere Stabilitäten als Cäsiumstandards (relative Unsicherheit von 10^{-18} vs. 10^{-15}). Einer der Hauptbestandteile einer solchen Uhr ist ein Laser mit sehr schmaler Linienbreite. Als ersten Schritt in Richtung des Betriebs einer optischen Uhr in Österreich, wurde im Zuge des EMPIR Projektes „Coulomb Crystals for Clocks“ (CC4C) vom Bundesamt für Eich- und Vermessungswesen, kurz BEV, ein solcher Laser beschafft. Des Weiteren wurde im Rahmen des Projekts zunächst die Schaffung einer Glasfaserverbindung von Wien nach Brünn evaluiert und im weiteren Verlauf des Projekts auch hergestellt, um eine Vergleichsmessung des ultra-stabilen Lasers am BEV mit dem Pendant des „Institute for Scientific Instruments“ (ISI) in Brünn durchführen zu können.
Diese Arbeit beschäftigt sich, nach kurzer Einführung in die Grundlagen, mit der Charakterisierung des Driftverhaltens, der Zero-Crossing Temperatur und der Frequenzstabilität des Lasers und der Erstellung eines Unsicherheitsbudgets. Zur Erstellung der Daten wurden unter anderem Vergleichsmessungen mit dem ISI in Brünn herangezogen.

Abstract

After more than half a century as primary frequency standard caesium clocks have exhausted their potential to improve their stability. Therefore, a replacement by a new standard that is even more precise is imminent. The potential successor standards are optical clocks, which use energy level transitions that produce electromagnetic waves in the optical regime of the frequency spectrum. These optical clocks achieve significantly higher stabilities than cesium standards (relative uncertainty of 10^{-18} vs. 10^{-15}). One of the main components of such a clock is a laser with a very narrow line width. In the framework of the EMPIR project "Coulomb Crystals for Clocks" (CC4C), the Federal Office for Metrology and Surveying (BEV) acquired such a laser as a first step towards the operation of an optical clock in Austria. Furthermore, as part of the project, the installation of a fiber optic connection from Vienna to Brno was initially evaluated and, in the further course of the project, it was also established in order to be able to carry out a comparison measurement of the ultra-stable laser at the BEV with its counterpart of the "Institute of Scientific Instruments" (ISI) in Brno.
After a short introduction to the matter, this thesis deals with the characterization of the laser's drift behavior, frequency stability, the cavity's zero-crossing temperature and the creation of an uncertainty budget. The collected data includes results from comparison measurements with the ISI in Brno.

Contents

CHAPTER 1

Introduction

1.1 Time and Frequency

Time might be, together with length and mass, the most intuitively perceptible physical quantity. While the other two quantities form the basis for what surrounds us, time enables the universe to evolve. But also much less philosophically, time is an essential quantity in everyday business life, social life and science. The unit of time in the *Système international d'unités* (SI) is the second and it is defined as:

> "The second, symbol s, is the SI unit of time. It is defined by taking the fixed numerical value of the caesium frequency $\Delta\nu_{\mathrm{Cs}}$, the unperturbed ground-state hyperfine transition frequency of the caesium 133 atom, to be 9 192 631 770 when expressed in the unit Hz, which is equal to s^{-1}." [Gen18]

As the definition suggests, the primary realisation of the second is a caesium clock, in which Cs atoms travel through a microwave resonator and are excited from the hyperfine state $F = 3$ with $m_F = 0$ to the hyperfine state $F = 4$ with $m_F = 0$ and then detected. The resonator's frequency is adjusted to the value where the signal at the detector is at its maximum. There are several effects like the second-order Doppler shift, gravitational shift, shifts from magnetic fields, et cetera that shift the energy levels in the atom and, hence, the transition's frequency from the unperturbed value. These shifts need to be mitigated and accounted for. Most of these effects are small or can be well compensated for the transition that is used in caesium clocks. The caesium clock fulfills its role as a reliable, stable and affordable realisation of the second very well. Hence, the current realisation of the second has endured for more than half a century by now (first used as realisation of the second in 1967). The most sophisticated microwave frequency standard is the caesium fountain clock, which has a fractional uncertainty of around 10^{-15} [Rie06]. However, this uncertainty is achieved after averaging over a day. In terms of short-term

stability (averaging time of seconds) there are several frequency standards that provide better uncertainty than caesium clocks, for instance hydrogen masers and optical clocks. In recent years the latter have started to surpass caesium clocks not only in short-term stability (10^{-13} vs. 10^{-15}), but also in long-term stability (10^{-15} vs. 10^{-18}) [MS21]. In a strategy document by the Consultative Committee for Time and Frequency from 2016 a number of milestones were set that have to be achieved in order to warrant a redefinition of the second [fTF16]. Although some of the milestones, for example in terms of stability performance and clock comparisons, have been reached, the given earliest date of redefinition, 2026, seems quite ambitious at this point.

1.2 Lasers as frequency standards

The considerable advantage of lasers over microwave oscillators is their higher frequency. The optical regime is in the range of several hundred THz, whereas the frequency of microwaves is in the range of GHz. This advantage is twofold: First, the higher an oscillator's frequency, the higher its quality factor $Q = \frac{\nu}{\Delta\nu}$, with $\Delta\nu$ being the line width. A high Q is desirable, because it is proportional to the oscillator's frequency uncertainty. Second, a high frequency allows faster comparison of two oscillators, hence, resulting in shorter averaging times for measurements. For example, to reach a fractional uncertainty of 10^{-15} with a microwave oscillator takes hours of averaging time, while it only takes seconds with an optical oscillator.
The typical set-up for a highly stable oscillator in the optical regime consists of a laser with low phase noise that is locked to an external Fabry-Pérot cavity to further reduce its phase noise (this topic will be treated in more detail in chapter 3). In an optical clock such an ultra-stable laser system is used as probing laser that is locked to the transition frequency of an atom or an ion. In order to keep this transition frequency as narrow as possible one has to inhibit the movement of the clock atoms/ions (see fig. 1.1). To achieve this suppression of movement, the clock atoms/ions are laser-cooled. To eliminate the residual motion there are two techniques to trap the atoms/ions, which divide optical clocks into two types: lattice clocks and single ion clocks. The former uses lasers, operated in such a way that standing waves occur, which in turn form a lattice of potential wells. In these potential wells atoms accumulate and are confined to a smaller space. In single ion clocks, an individual ion is trapped in an electromagnetic field. Both types have advantages and disadvantages, however, the lattice clocks appear to have a slight edge because of the high number of emitters that can be trapped.
The obtained optical frequency is too fast for current electronics and cannot be counted directly. Therefore, a frequency comb generator, which is a mode-locked femtosecond laser, is used to transfer the frequency from the optical into the RF regime (e.g. 10 MHz) (for more information see [UHH02]). In figure 1.1 the necessary parts for an optical clock are summarised in a schematic.
It is important to be able to compare optical oscillators, even over large distances. Especially, since more and more optical clocks are supposed to contribute to the international atomic time (TAI). Nowadays most of the contributing clocks are microwave standards

and are compared via satellites. However, this comparison technique is not suitable for the needed accuracy of optical clocks (10^{-18}). Phase-coherent fiber links provide a feasible alternative.

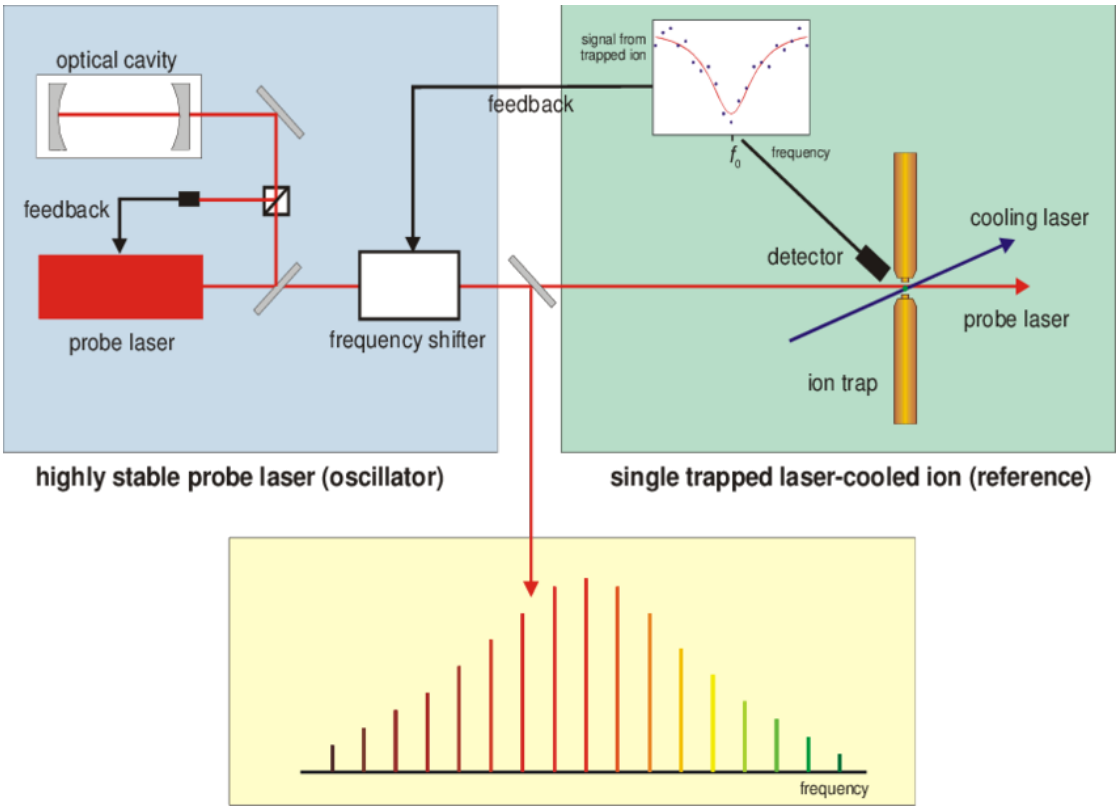

Figure 1.1: Schematic of an ion optical clock setup [GBK+21].

1.3 Outline

After a short introduction to the theoretical background on fundamental phenomena regarding cavities, Allan variance and second harmonic generation in chapter 2, an overview over the used ultra-stable laser system is given in chapter 3. In chapter 4 the operated and planned fiber links are described. In chapter 5 the performed measurements are presented and, finally, in chapter 6 conclusions and an outlook are given.

CHAPTER 2

Theoretical Background

2.1 Optical Resonator

An optical resonator and the standing waves it produces inside, can be used as a reference for a laser. In its simplest form is made up of two reflective surfaces. The cavity used in this work is a hemispherical resonator, i.e. a resonator with one plane mirror and one concave mirror. If we look at an optical resonator from the idealised perspective of ray optics, the problem is quite simple, and the basic principles can be clearly demonstrated. The smallest possible mode in the resonator with length L has a frequency of $f = \frac{c}{2L}$ (see fig. 2.1a), because only standing waves are reasonably stable over time. The electromagnetic wave between the mirrors will gradually suffer energy losses due to imperfect reflectivity of the mirrors (fig. 2.1c). Therefore, the mode will decay exponentially with some rate $\frac{1}{\tau}$, which is directly proportional to the losses and approximately the mode's linewidth $\Delta f \approx \frac{1}{\tau}$ (fig. 2.1b). If there were no losses at all in the resonator, the contribution to the mode's linewidth would be zero and the frequency would resemble a delta function. So, the lower the losses the narrower the linewidth. One can achieve a narrower linewidth by either compensating the losses with a gain medium, which is done in lasers, or by improving the mirror's reflectivity. The latter is done in external cavities, however, there is a certain limit to maximising the reflectivity R, because light has to be injected into the resonator, which is not possible if $R = 1$ and, hence, the transmission T equals zero.

An optical resonator can accommodate many modes, as long as their frequencies meet the following boundary condition:

$$\lambda_n = \frac{2L}{n}, \text{ resp.} \tag{2.1}$$

$$f_n = n \cdot \frac{c}{2L}, \tag{2.2}$$

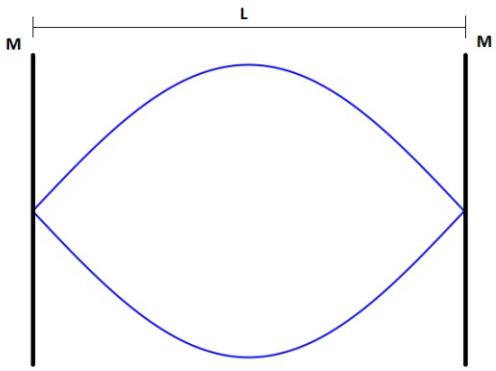

(a) Smallest stable longitudinal mode between two mirrors that are a distance of L apart. Its wavelength is twice the resonator's length.

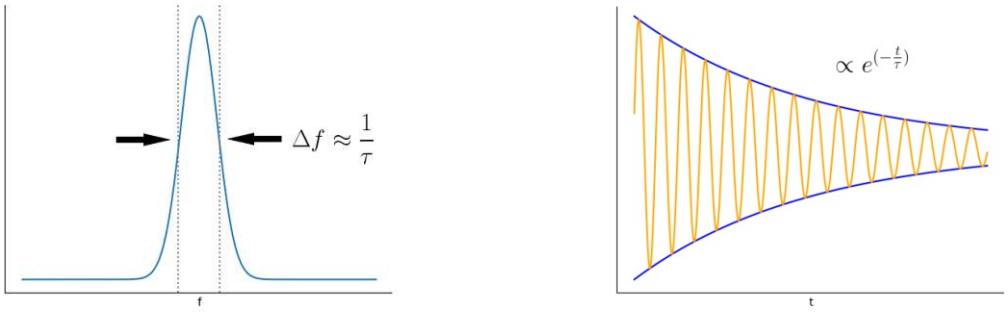

(b) (c)

Figure 2.1: Due to imperfect reflectivity of the resonator's mirrors the electromagnetic waves suffer power losses and decays exponentially with a rate of $\frac{1}{\tau}$, which can be seen in (c). The resulting linewidth corresponds to approximately the rate of decay (b).

with n being the mode number (see fig. 2.2). Because the resonator only allows certain, discrete longitudinal modes with finite linewidth, there is a spacing of $\frac{c}{2L}$ between the modes. This distance is called the free spectral range (FSR). Beside longitudinal modes there are also transverse modes that have to be taken into account. Usually one wants to have a single spot with a Gaussian power distribution, which corresponds to the TEM00 mode. This mode is favourable, because it confines all of the power in one area, in contrast to all higher modes that consist of several spots (fig. 2.3a). These modes have a different optical path in the cavity, therefore their frequency is slightly different from that of the TEM00 mode. For reference see the excellent lectures of Prof. Shaoul Ezekiel [Sha08].

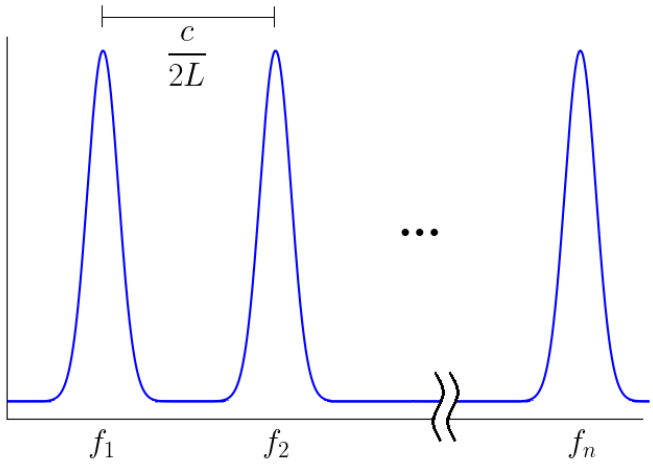

Figure 2.2: Frequency picture of several modes in a resonator equidistantly spaced by the free spectral range.

For optical resonators that are used as an external cavity, in order to reduce the linewidth of a laser, the reflectivity/transmission is an important quantity. In this case the cavity can be described as a Fabry-Perot interferometer, which consists of two plane mirrors between which the light waves bounce back and forth and pass the cavity only if they are in resonance with the interferometer, i.e. fulfill condition (2.1). The transmission of

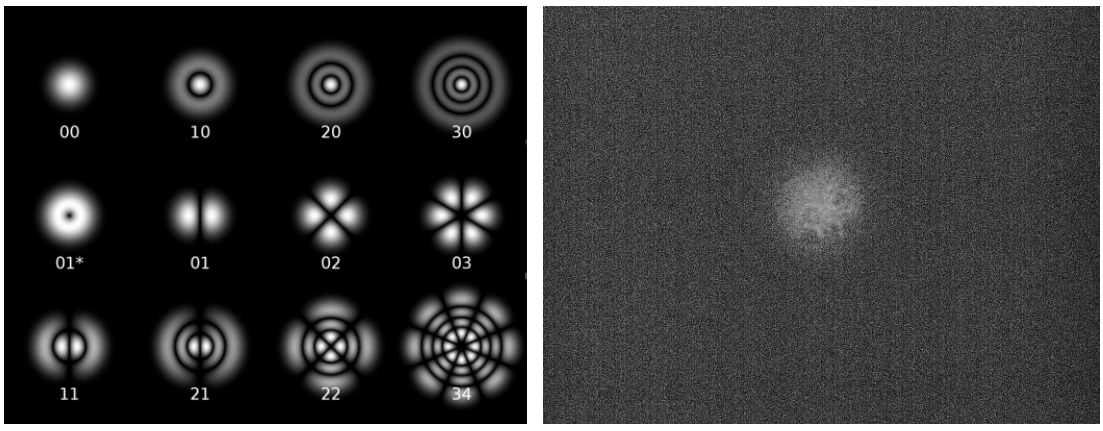

(a) (b)

Figure 2.3: (a) Transverse laser modes in a cavity with circular mirrors [Wik08]. (b) Picture of the TEM00 mode of BEV's ultra-stable laser system.

a Fabry-Perot interferometer is given by the following formula:

$$T = \frac{1}{1 + F \sin^2(\frac{\delta}{2})} \tag{2.3}$$

where

$$F = \frac{4r^2}{1 - r^4} \tag{2.4}$$

is the coefficient of finesse which is proportional to the finesse and r is the electric field reflectivity. δ describes the phase difference between two rays in the resonator

$$\delta = \frac{4\pi n L}{\lambda} \cos(\theta). \tag{2.5}$$

In fig. 2.4 a Fabry-Perot cavity's transmission is plotted as a function of δ for two different values of reflectivity. The higher the reflectivty of the mirrors, the higher is the cavity's finesse and, hence, the narrower are the transmitted peaks. The finesse describes the ratio of the FSR to the linewidth:

$$\text{Finesse} = \frac{f_{\text{FSR}}}{\Delta f}. \tag{2.6}$$

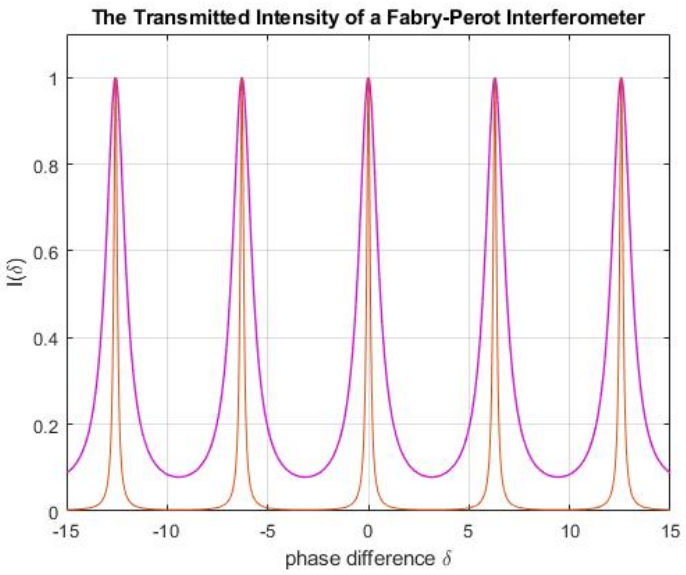

Figure 2.4: A Fabry-Perot cavity's transmission as a function of phase difference δ for a power reflectivity of 0.75 and 0.95. These values roughly correspond to finesse values of 5 respectively 30. The cavity used in the ORS has a finesse of 320000 and the peak profile is very close to a delta-function. The picture was created with a Matlab script based on the code in this reference [Sul15].

2.2 Zero-crossing Temperature

As mentioned previously, cavities can be used to lock a laser's frequency to the cavity's resonance frequency. The resonance frequency changes with cavity length, i.e. thermal expansion. So for a good lock performance, the cavity's length changes due to temperature have to be kept at a minimum. Certain types of materials have a temperature, where their coefficient of thermal expansion (CTE) crosses zero; e.g. water and also ultra low expansion (ULE) glass. Below this point the material contracts when heated and above this point the material expands when heated. When a cavity is kept at this "zero-crossing temperature" its length changes due to thermal expansion are the smallest.

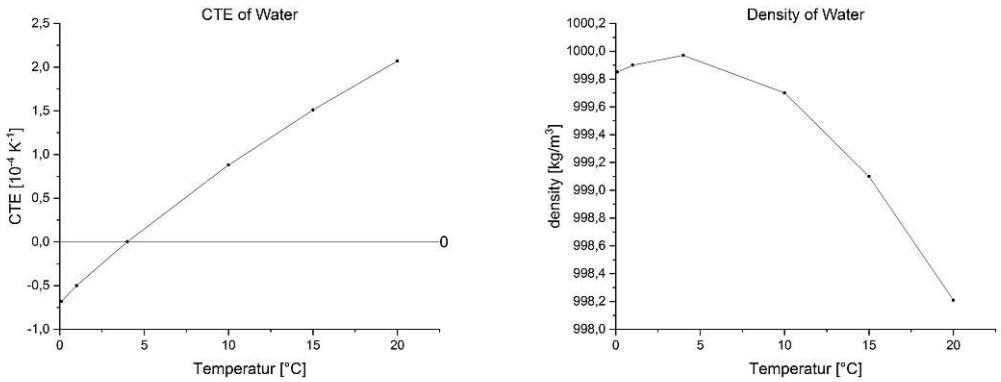

(a) (b)

Figure 2.5: Graphs of the CTE and density of water. Because of the CTE's zero crossing there is a maximum in the density plot. In section 5.3 we will see this extremum in a frequency plot, due to the relationship of a cavity's length and its modes' frequencies.

ULE glass has a CTE of $3 \times 10^{-8}\,\mathrm{K}^{-1}$ [Cor]. For a cavity that is 12.1 cm long, this means that a change of 1 Kelvin results in a change in cavity length of 3.6 nm. For a wavelength of 1550 nm this translates to a change of 0.05 pm in wavelength respectively roughly 6 MHz in frequency.

2.3 Allan Variance

The Allan variance, or its root the Allan deviation, is used as a measure for the stability of an oscillator. It is determined by comparing two oscillators, where one of them usually acts as a reference to which the other oscillator is compared. It is defined as:

$$\sigma_y^2(\tau) = \left\langle \sum_{i=1}^{2} \left(\bar{y}_i - \frac{1}{2} \sum_{j=1}^{2} \bar{y}_j \right)^2 \right\rangle = \frac{1}{2} \left\langle (\bar{y}_2 - \bar{y}_1)^2 \right\rangle, \tag{2.7}$$

where

$$\bar{y}_i = \int_{t_i}^{t_i+\tau} y(t)dt, \tag{2.8}$$

with τ being the measurement time and

$$y(t) = \frac{\Delta\nu(t)}{\nu_0} \tag{2.9}$$

being the fractional frequency deviation. The main difference of the Allan deviation in comparison to the standard deviation is that it describes the difference between adjacent frequency values instead of the difference of a frequency value to the mean. For reference see [Rie06]. The Allan deviation is usually given as a plot for several values of τ as shown in fig. 5.6a. From the slope of the Allan plot one can obtain information about the different kinds of noise on the signal. There are several versions of the Allan deviation that serve different purposes, e.g. the so-called "modified Allan deviation" where white phase modulation and flicker phase modulation have a different slope in the Allan plot and, hence, can be distinguished, which is not possible in the original Allan deviation.

2.4 Second Harmonic Generation

In order to link BEV's traceable frequency source to the experiments at ATI, the transferred laser light has to be frequency doubled (see section 4.2). This is done with a technique called second harmonic generation. Second harmonic generation is a process that uses the non-linear properties of a material's polarisation function

$$P(E) = \epsilon_0 \left[\chi^{(1)}E + \chi^{(2)}E^2 + \chi^{(3)}E^3 + ...\right] \tag{2.10}$$

to generate light with double the frequency with respect to the incoming light. Looking at the quadratic term in (2.10)

$$P_i = \epsilon \sum_{j,k=1}^{3} \chi^{(2)}_{i,j,k} E_j E_k, \qquad i,j,k = 1,2,3 \tag{2.11}$$

and considering a superposition of two waves E_1 and E_2, the following product terms $E_i E_j$ will arise:

$$\begin{aligned}(E_1 + E_2) &= E_{01}^2 \cos^2 \omega_1 t + 2E_{01}E_{02} \cos\omega_1 t \cos\omega_2 t + E_{02}^2 \cos\omega_2 t \\ &= \frac{E_{01}^2}{2}(1 - \cos 2\omega_1 t) + \frac{E_{02}^2}{2}(1 - \cos 2\omega_2 t) \\ &+ E_{01}E_{02}\left[\cos(\omega_1 - \omega_2)t - \cos(\omega_1 + \omega_2)t\right].\end{aligned} \tag{2.12}$$

In equation (2.12) terms with the doubled frequencies $2\omega_1$, $2\omega_2$ and the sum and difference frequency occur. In case that $\nu_1 = \nu_2$, one speaks of second harmonic generation, where two photons of frequency ν combine to one photon with the doubled frequency $\nu_3 = 2\nu$. This will be the relevant process in section 4.2.
One important factor that has to be considered in SHG is phase matching. The polarisation wave created in the crystal by the incident light (ω_{fund}), travels through the crystal with the same velocity as the incident light. This velocity is determined by the index of refraction $n(\omega_{\text{fund}})$. The value of the refractive index generally depends on the frequency of the light. The polarisation wave creates light with two times the frequency of the fundamental light $\omega_{\text{harm}} = 2\omega_{\text{fund}}$. Hence, its phase velocity $v = \frac{c}{n(\omega_{\text{harm}})}$ will be different. The phase of already created second harmonic light and newly created second harmonic light, which follows the phase of the fundamental light, will sinusoidally fall in and out of phase. After a distance called the coherence length the frequency doubled waves are in phase they will positively interfere and after twice this distance they are out of phase and will annihilate. Hence, one has to match the phase of ideally all created photons to receive the maximum yield. One way of realising this is so-called critical phase matching, where one uses a uniaxially birefringent crystal, which has two eigenmodes of polarisation, called the ordinary and extraordinary beam. The refractive index of the ordinary beam n_o is isotropic. The extraordinary beam's refractive index n_e, however, is dependent on the incident angle of light. If one guides light through the crystal at a critical angle, the refractive index of the frequency doubled extraordinary beam $n_e(2\omega)$ will be equal to

the refractive index of the ordinary, fundamental wave $n_o(\omega)$ (see fig. 2.6a). With both refractive indices being the same, the phase of the fundamental wave and the second harmonic wave will match along the crystal. The electric field of the second harmonic will increase linearly and its power quadratically. A downside to this technique is that the phase matching condition can only be realised for a limited range of frequencies. With a method called quasi phase matching, one can extend this range of frequencies. Here, the crystal's polarisation is periodically modulated in such a way that its direction changes every multiple integer of the coherence length. So, after each distance where the second harmonic reaches its plateau of positive interference, and the waves would start to annihilate, the change of direction in polarisation introduces a phase shift of π and, hence, back into the range of positive interference. For reference see [Rie06].

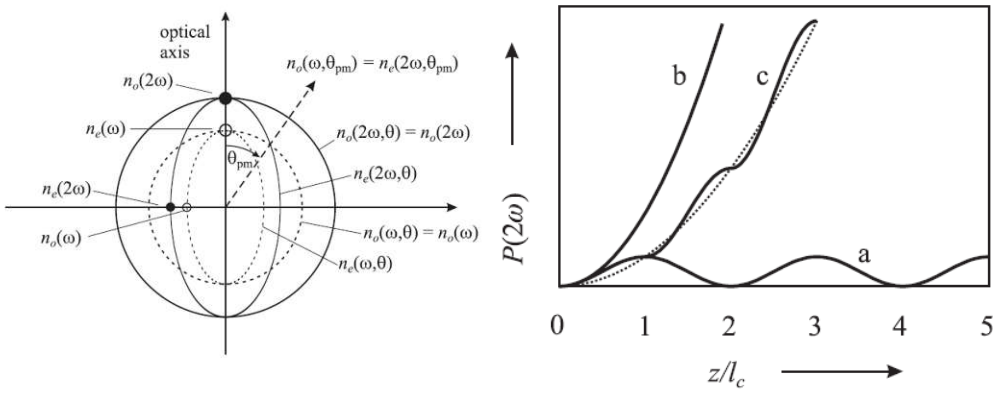

Figure 2.6: (a) Magnitude of the refractive index as a function of angle of incident. The refractive index of the ordinary beam is isotropic and therefore a circle in this graph. The extraordinary beam's refractive index depends on the angle of incident θ and forms an ellipse. If the angle of incidence coincides with the optical axes, the refractive indices are the same for both beams. The crossing point between the ellipse of $n_o(2\omega)$ and the circle of $n_e(\omega)$ defines the phase matching condition $n_o(2\omega) = n_e(\omega)$. [Rie06]
(b) This picture shows the second harmonic's power function without phase matching in "a", critical phase matching in "b" and quasi phase matching in "c". [Rie06]

2.4.1 Optical Arrangement

The TEM00 mode of a laser has a Gaussian beam profile, which means that its amplitude envelope is given by a Gaussian function. In contrast to ideal ray optics, a Gaussian beam cannot be focused to a infinitely small spot, but only to a finite cross section with a certain beam waist w_0. The beam width as a function of propagated distance z is given as

$$w(z) = w_0\sqrt{1 + \left(\frac{z}{z_r}\right)^2}, \tag{2.13}$$

where

$$z_r = \frac{\pi w_0^2 n}{\lambda} \tag{2.14}$$

is the Rayleigh length. In section 4.2 a periodically poled Lithium Niobate (PPLN) crystal is used for second harmonic generation. For optimal conversion in the PPLN crystal the laser light has to be focused into the center of the crystal. Furthermore, the ratio of the length of the crystal to the confocal parameter ($b = 2z_r$) has to be 2.84 [BK68]. When choosing the focusing lens, one has to consider the different refraction indices of air and the crystal. The procedure for calculating the focal length of the lens and the required beam width after the collimator was to first calculate b from

$$\frac{l}{b} = 2.84, \tag{2.15}$$

which is 14.1 mm for a crystal length of 40 mm. With (2.14) one gets a beam waist w_0 of 40.3 µm. With (2.13) one can calculate the beam width at the edge of the PPLN crystal and consequently the beam width at the focusing lens. For example with a lens with a focal length of 50 mm, the beam width at the lens and, hence, also after the collimator decoupling the light from the fiber, is around 0.5 mm, which corresponds to a beam diameter of 1 mm.
An overview of this topic can be found in [Edm] and [Cov].

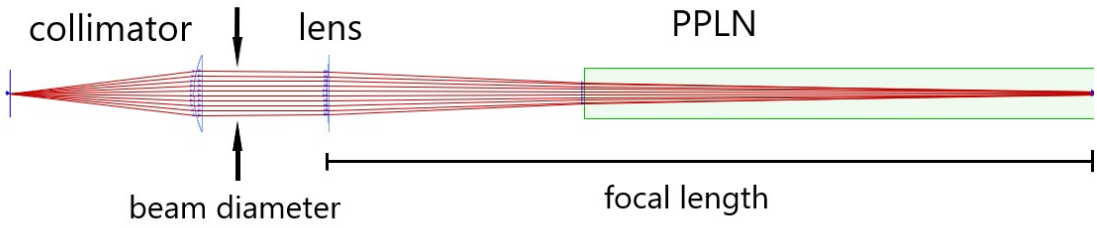

Figure 2.7: The relevant parts of the optical arrangement for second harmonic generation with a PPLN crystal. Half the crystal is depicted in green and the focusing lens in blue. The ratio of the length of the crystal to the confocal parameter is given by [BK68]. From the confocal parameter one can calculate a suitable focal length - beam diameter combination. The schematic was drawn with the programme OpticalRayTracer [Lut17].

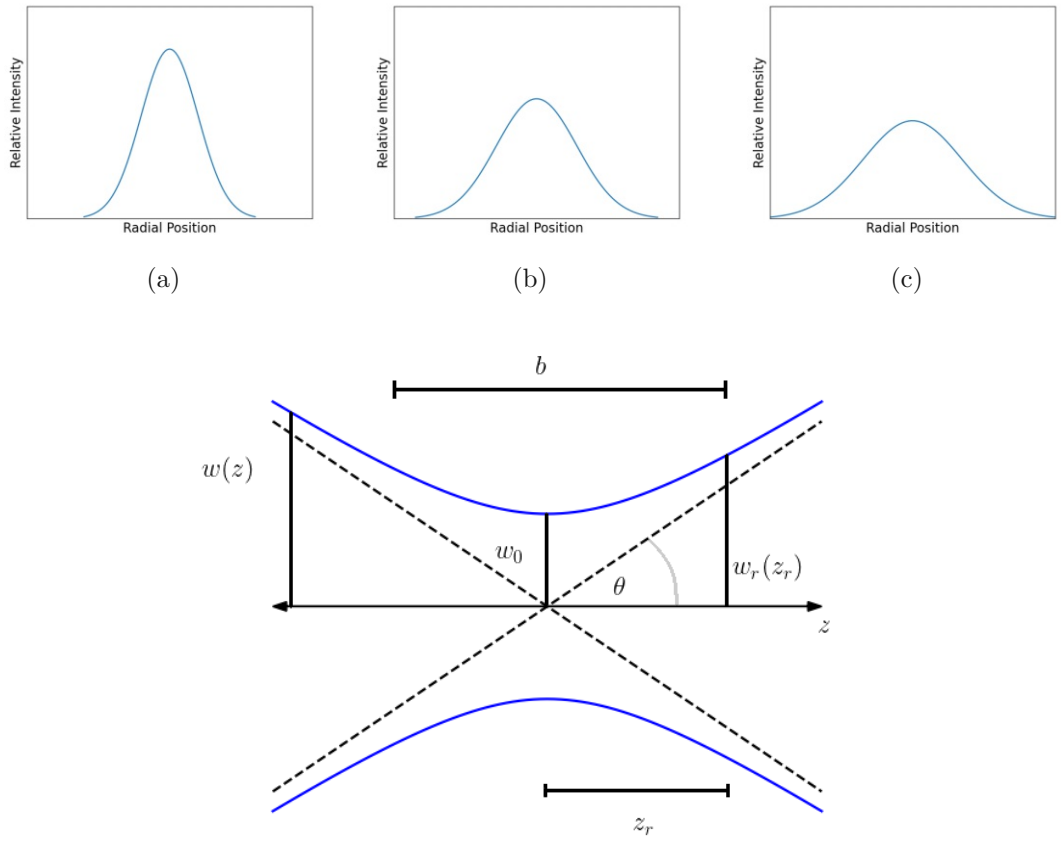

Figure 2.8: Pictures (a) to (c) show a Gaussian beam profile diverging while propagating in z direction. In (d) the smallest cross section is marked as w_0 and is called beam waist. After the Rayleigh length z_r the beam width increases to $w_r = \sqrt{2}w_0$. The parameter $b = 2z_r$ is called the confocal parameter.

CHAPTER 3

Ultra-stable Laser System

The ultra-stable laser is a so-called "Optical Reference System 1500" (ORS1500) made by Menlo Systems [Mena]. The ORS contains a RIO Planex Laser Diode that is stabilized with an external cavity (length = 12.1 cm) by a Pound-Drever-Hall (PDH) locking system (fig. 3.1). It operates at a wavelength of 1542.14 nm, which corresponds to a frequency of roughly 194.4 THz. This wavelength was chosen in order to match the ITU-T DWDM channel 44 [ITU20] for optimal transfer conditions via glass fiber. The ORS is very sensitive to vibration and temperature fluctuations, hence, the cavity and the optics are in a temperature stabilised chamber. This chamber rests on an aluminium frame that was built to protect the ORS from floor vibrations (fig. 3.2). Additionally, the optics and the cavity are set up on an active vibration isolation platform. The surrounding rack with the electronics is supported by a separate set of wheels.

3.1 Laser

The laser diode already has a fairly narrow linewidth of 2.8 kHz (Lorentzian FWHM). However, for clock operation the desired linewidth is in the sub-Hertz range, so the laser is locked to an external cavity to suppress the noise level even further, resulting in a sub-Hertz linewidth. The output power of the RIO Planex is 20 mW and the output power of the stabilised light is 8 mW.

3.2 Locking Mechanism

The Pound-Drever-Hall Locking technique creates an error signal by mixing the beat note from a laser's reflection off a cavity and a side-band that was modulated onto the laser's light with an EOM and an RF signal from a local oscillator. This error signal is fed to the laser's actuators[1] via a loop filter to keep the laser's frequency as close to the resonance

[1] The laser current acts as the fast actuator and the laser temperature control is the slow actuator.

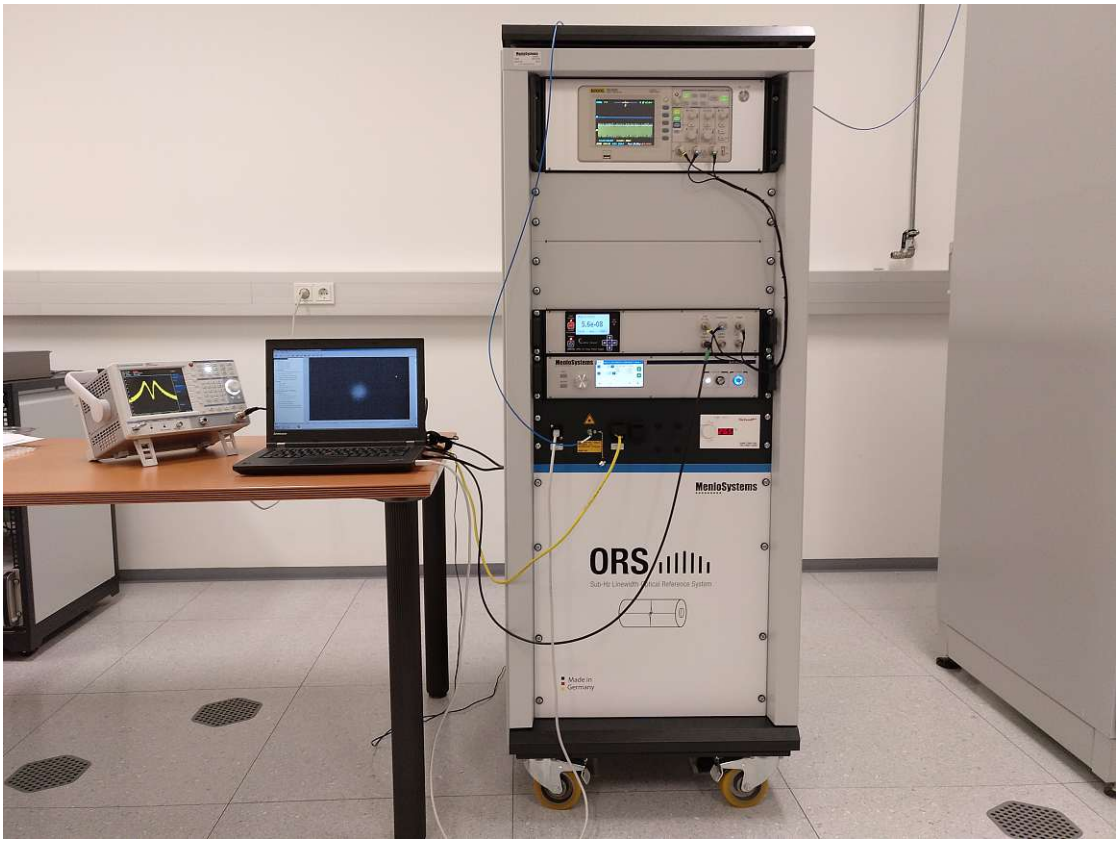

Figure 3.1: Picture of the ORS shortly after its arrival in 2018.

of the external cavity as possible. The main advantage of this locking mechanism is that the error signal generation is theoretically independent of power fluctuations produced by the laser.

The following discussion of the PDH locking scheme follows along the derivation in the introductory paper by Eric Black [Bla00]. As seen in fig. 3.3 a part of the laser's output is guided through an electro-optic modulator (EOM), where the laser light is phase modulated with an RF frequency Ω_m:

$$E_{inc} = E_0 e^{i(\omega t + \beta \sin(\Omega_m t))}. \tag{3.1}$$

Due to the birefringence of the crystal in the EOM, care must be taken that the polarization of the input beam and the principal axes of the crystal are aligned. A misalignment will give rise to a residual amplitude modulation (RAM), which will be discussed below in section "Residual Amplitude Modulation - RAM". Equation (3.1) can

Figure 3.2: Aluminium pedestal to decouple the ORS from vibrations on the laboratory's floor.

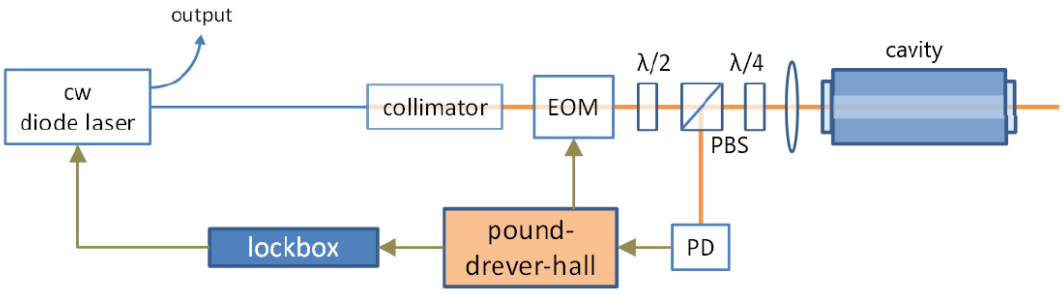

Figure 3.3: Schematic of the ORS1500 PDH locking system. [Men18]

be expressed with Bessel functions as

$$E_{inc} \approx [J_0(\beta) + 2iJ_1(\beta)\sin(\Omega_m t)]\, e^{i\omega t} \tag{3.2}$$

$$= E_0 \left[J_0(\beta)e^{i\omega t} + J_1(\beta)e^{(\omega+\Omega_m)t} - J_1(\beta)e^{(\omega-\Omega_m)t} \right]. \tag{3.3}$$

So the result is the original frequency of the laser at the center flanked by a sideband above and below at a distance of the modulation frequency Ω_m. The modulated frequency

passes a polarising beam splitter (PBS) and a quarter wave plate before reaching the cavity. The reflected light from the cavity will pass the quarter wave plate twice, which effectively let's it act as a half wave plate that rotates the polarisation in such a way that the light is reflected at the PBS towards the photo detector. Almost all of the total power of the incident beam $P_0 = |E_0^2|$ is distributed to the carrier $P_C = J_0^2(\beta)P_0$ and each of the first order sidebands $P_S = J_1^2(\beta)P_0$. In total

$$P_C + 2P_S \approx P_0. \tag{3.4}$$

With the reflection coefficient $F(\omega)$ the reflected power is

$$\begin{aligned} P_{ref} = {} & P_C\,|F(\omega)|^2 + P_S\left\{|F(\omega+\Omega_m)|^2 + |F(\omega-\Omega_m)|^2\right\} \\ & + 2\sqrt{P_C P_S}\left\{Re\left[F(\omega)F^*(\omega+\Omega_m) - F^*(\omega)F(\omega-\Omega_m)\right]\cos(\Omega_m t)\right. \\ & \left. + Im\left[F(\omega)F^*(\omega+\Omega_m) - F^*(\omega)F(\omega-\Omega_m)\right]\sin(\Omega_m t)\right\} \\ & + (2\Omega_m \text{ terms}). \end{aligned} \tag{3.5}$$

The detector sees terms of constant power, two terms that oscillate with the modulation frequency Ω_m, which will be the ones of interest, and terms with $2\Omega_m$. In case $\Omega_m \gg \omega_{\mathrm{FSR}}$, $F(\omega \pm \Omega_m)$ is -1 because the sidebands are totally reflected when the laser is near or in resonance with the external cavity. Hence, the expression $[F(\omega)F^*(\omega+\Omega_m) - F^*(\omega)F(\omega-\Omega_m)]$ is purely imaginary and only the sinus in (3.5) survives. The output of the photo diode is mixed with a radio frequency of Ω_m from a local oscillator[2] resulting in a product of two sines with either the sum or the difference frequency.

$$\sin(\Omega t)\sin(\Omega' t) = \frac{1}{2}\left\{\cos\left[(\Omega-\Omega')t\right] - \cos\left[(\Omega+\Omega')t\right]\right\}. \tag{3.6}$$

Since both inputs, the local oscillator (Ω') and the laser (Ω), have contributions with the same frequency Ω_m this product will be a DC signal ($\cos(0)$), which is isolated with a low-pass filter. The result is an error signal (fig. 3.4)

$$\epsilon \approx -\frac{4}{\pi}\sqrt{P_C P_S}\frac{\delta\omega}{\delta\nu} \tag{3.7}$$

where $\delta\nu$ is the cavity's linewidth and $\delta\omega$ is the deviation of the laser frequency from the cavity's resonance. Close to the resonance the error signal can be approximated as a linear function

$$\epsilon = D\delta f \tag{3.8}$$

with

$$D = -\frac{8\sqrt{P_C P_S}}{\delta\nu}. \tag{3.9}$$

[2]The signal coming from the local oscillator is phase shifted to compensate unequal delays on the two signal paths.

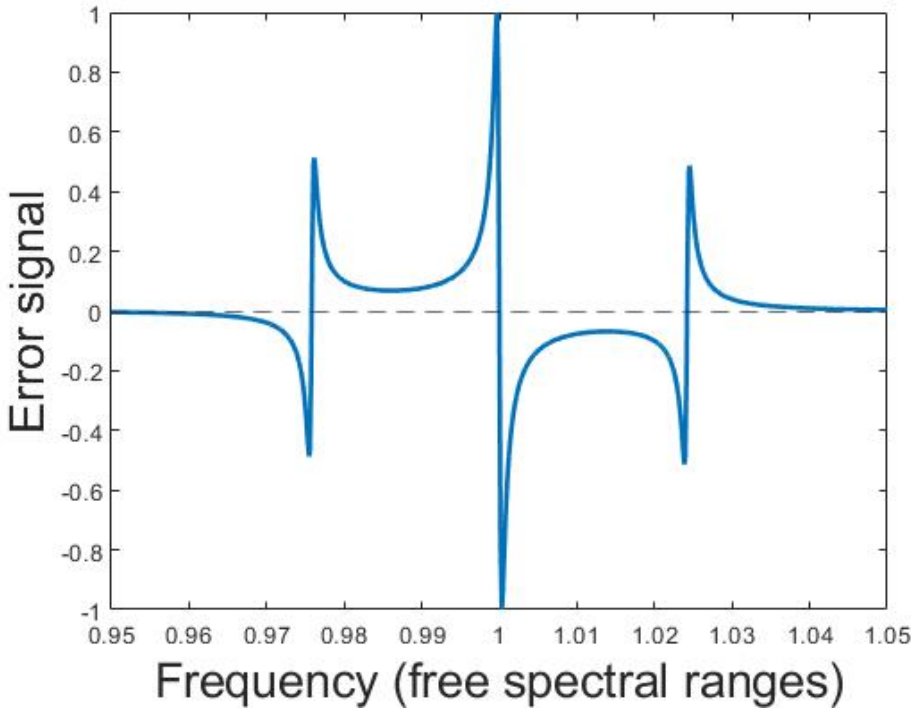

Figure 3.4: PDH error signal.

The steeper the slope D, the better the lock performance. D, on one hand, depends on the cavity linewidth and on the other hand on the ratio of the power in the sideband to the power in the carrier. As stated in [Rie06] the optimal ratio is $\frac{P_S}{P_C} = 0.42$ which corresponds to a modulation depth[3] β of 1.08. The error signal is fed to the fast actuator (laser current) and the slow actuator (laser temperature) via an PIID controller. With this locking technique the laser's linewidth is slimmed down from the kHz range to a sub-Hertz linewidth.

3.2.1 Residual Amplitude Modulation - RAM

As mentioned earlier, in principle, the PDH locking scheme is not susceptible to error signal noise due to fluctuations in laser amplitude, as it is locked to a minimum of the reflected power. However, temperature fluctuations of the EOM can give rise to RAM that oscillates with the modulation frequency. Therefore, this RAM passes the mixer and contributes to the error signal, resulting in an offset to the actual minimum of reflected power. It originates from the birefringent properties of the electro-optic crystal in the EOM. If the polarisation of the laser light is not aligned with one of the principle

[3]The modulation depth is a measure that describes how much the modulated variable varies around the unmodulated value.

axes, the polarization components experience different phase shifts that are modulated with the modulation frequency. The PBS after the EOM will then convert the phase modulation into an amplitude modulation. In practice it is very difficult to achieve a perfect alignment due to vibrations and temperature fluctuations. There are some techniques to suppress RAM ([ZMB+14]), e.g. by taking two crystals that are rotated in such way that the phase shifts, caused by the crystals due to polarization, cancel each other or actively suppressing the RAM with a control loop that modifies the modulation frequency.

3.3 Cavity

The external high-finesse (320000) cavity is made from ultra low expansion glass (ULE) and has a length of 12.1 cm which roughly corresponds to a FSR of 1.24 GHz. The cavity is kept at a steady temperature with a thermoelectric cooler (peltier element). As mentioned in section "Locking Mechanism" the cavity is the dominating source of instability in the frequency. Hence, it has to be protected from environmental influences. Therefore, the cavity is within a vacuum chamber with a pressure of 8×10^{-9} mbar to suppress vibrations and heat transfer. The working vacuum pressure is maintained with an ion getter pump. To minimise the contact surface, the cavity rests on four small rubber balls. In order to keep the influence of thermal expansion at minimum, the cavity is kept at the so-called zero-crossing temperature (section 2.2). However, no matter how well a cavity is isolated, there will always be a continuous change in length due to aging - the amorphous material, the cavity is made of, shrinks over time. This results in a (nearly) linear drift in frequency. Furthermore, this drift decreases over long periods of time, as the cavity ages (see section 5.1).

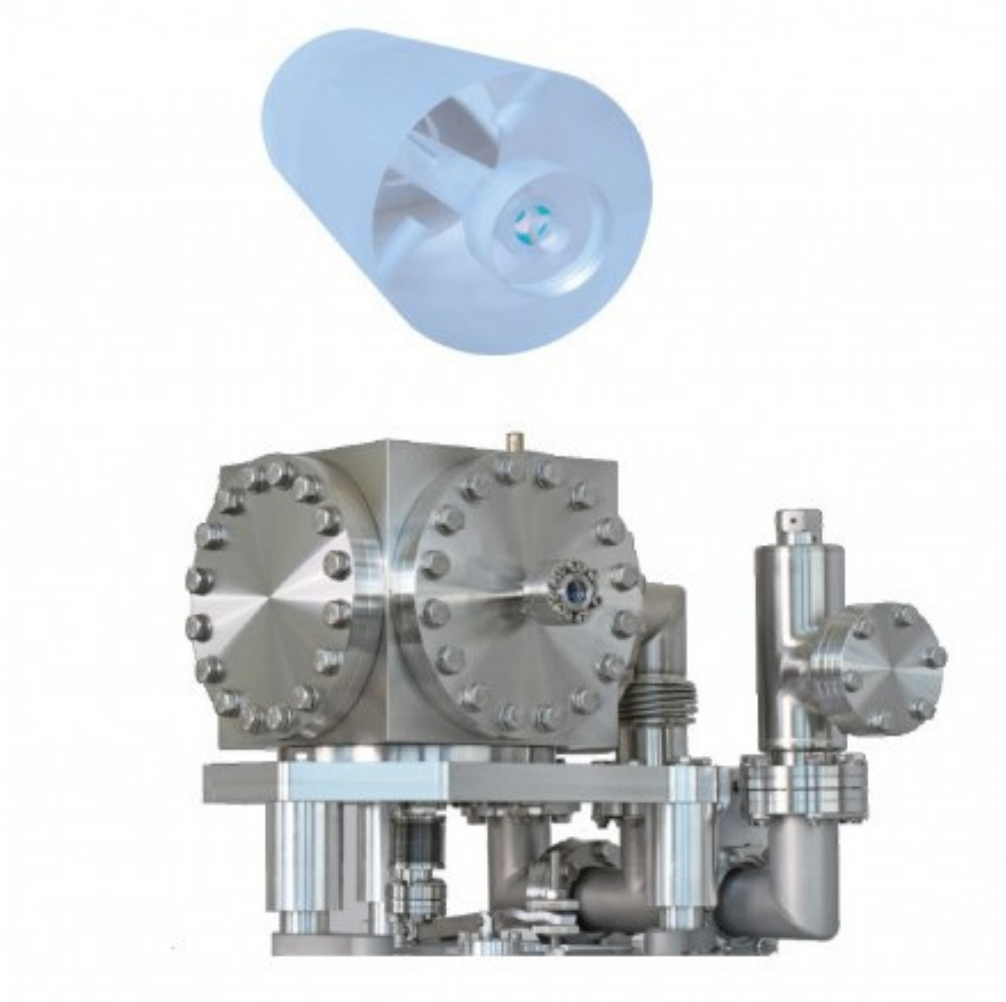

Figure 3.5: The ORS's cavity and its vacuum container [Menb].

CHAPTER 4

Fiber Links

Current atomic clocks, based on microwave transitions, are compared via satellites. This comparison technique, however, can only achieve a fractional frequency uncertainty of the order of 10^{-15} ([Rie06], chapter 12.5). Compared to the fractional uncertainties of optical clocks of 10^{-18}, current GPS measurement techniques are not an adequate technology for comparisons of optical clocks. A suitable alternative are phase-coherent fiber links.

4.1 Fiber link Brno

The stability of ultra stable lasers after averaging times of a few to several 100 seconds is at least two orders of magnitude better than RF oscillators. Therefore, it is not possible to measure the full stability potential of the ORS with a comb that is locked with RF reference signals. To further investigate the short term stability of the ORS it has to be compared with another ultra stable laser. As part of the EMPIR research project CC4C the ORS was compared to an ultra stable laser at the ISI in Brno. The ISI and BEV were connected via glass fiber. The used fiber is kept free from any other (commercial) traffic and is therefore called a "dark fiber". To compensate for the losses along the 240 km long fiber bi-directional amplifiers have to be used. For a meaningful comparison the fiber has to be phase-stabilised. A schematic picture of the link can be seen in figure 4.1. The two ultra stable lasers on both sides can be used as either master or slave laser in this configuration. As soon as the phase stabilisation of the link works satisfactory this will allow a transfer of information from and to both sides of the link via the ultra stable lasers. For example a comparison of the two H-masers is in preparation. The principle of the phase stabilisation is the same as in this paper [MJYH94]. As stated before, this link can work in both directions, so, for this discussion the Czech laser is declared as the master laser and the ORS as the slave laser. In the schematic the laser that is transferred from Brno to Vienna is called "Laser ISI 1542". It is a Koheras Basik Laser with narrow linewidth that is locked to a frequency comb, which is in turn locked to the ultra stable

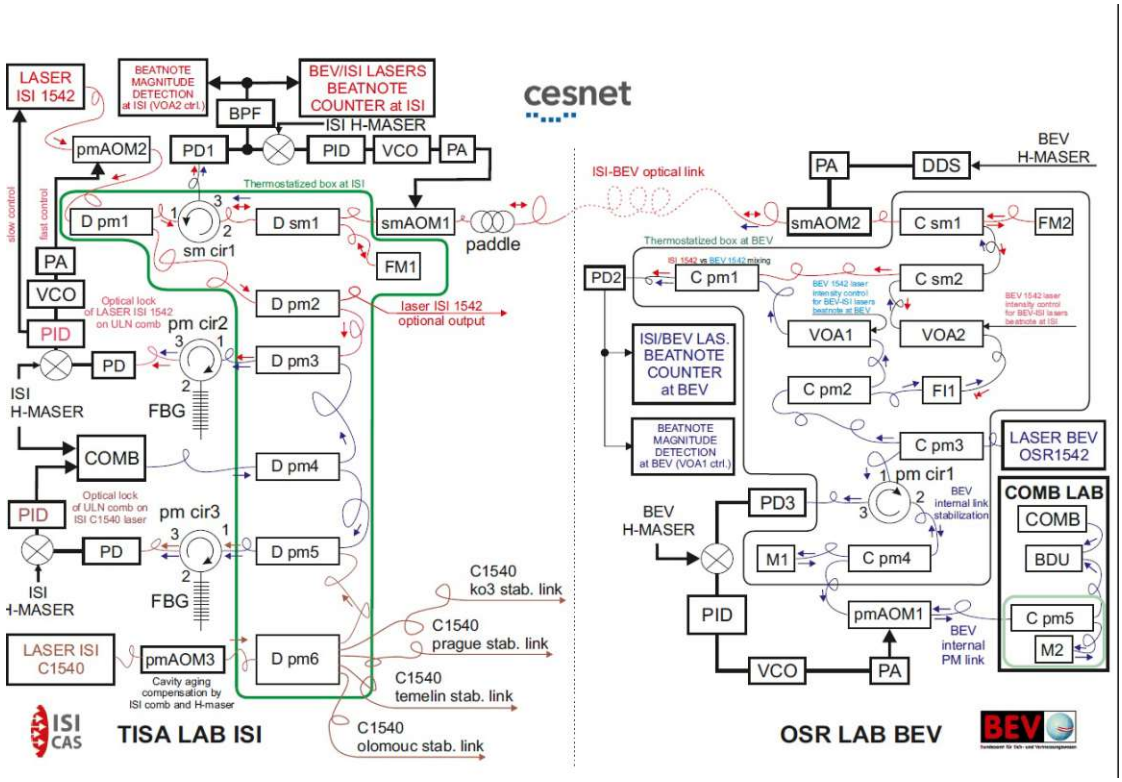

Figure 4.1: Schematic of the fiberlink and its stabilisation [Cip19].

laser at Brno ("Laser ISI C1540"). This has to be done because the ORS in Vienna is at 1542 nm while the ultra stable laser in Brno is at 1540 nm. This gap in wavelength is too large for a beating measurement (≈ 300 GHz). Therefore the stability of the "Laser ISI C1540" is transferred to the "Laser ISI 1542" via a lock to the frequency comb. The laser "Laser ISI 1542" passes a circulator "sm cir1" from port 1 to port 2 and a splitter "D sm1" before going through an AOM "smAOM1" that is driven with an radio frequency of 80 MHz. This AOM is the actuator for the control loop that compensates the phase noise collected along the fiber. The signal then enters the fiber link to Vienna. In the ORS laboratory the light first passes a manual fiber polarisation controller (paddels). Along the link the temperature around the fiber fluctuates and with it the polarisation of the light. The paddles help to rotate the polarisation of the signal from Brno to the desired angle for the measurement done in Vienna. Next in line is the second AOM "smAOM2" which modulates a constant 40 MHz onto the signal. This is done to mark the reflection at the end of the fiber link[1] and, thus, the correct signal for the beating measurement back in Brno can be identified. After the AOM the signal is split. The majority of the signal is directed to the experiments at BEV and the rest is reflected back

[1]The link consists of several connected fibers. On any of those connections, or parts in the link or sharp bends there could be (strong) reflections. These could be mistaken as the reflection from the end of the fiber and lead to wrong compensations of the control loop.

into the link with a Faraday mirror “FM2”. The light passes the two AOMs again and has now collected a total frequency shift of 240 MHz. In the splitter “D sm1” the light from the link is combined with the reflected light from mirror “FM1”. The combined light passes the circulator “sm cir1” from port 2 to port 3. The photodiode “PD1” detects the beat-note between the light from mirror “FM1” and from the round-trip along the fiber link. This beat is mixed with an RF signal from ISI’s H-maser to generate an error signal for a phase-locked loop (PLL). The PLL compensates the noise collected along the fiber link by shifting the transferred laser light with the AOM in such a way that the phase relation between the beat-note and the (multiplied) RF signal from the H-maser remains constant.
At this point in time the fiber link is active and the link stabilisation is working, as can be seen in figure 4.2. The settings of the compensation loop still have to be fine tuned for optimal lock performance. Measurements of the beat-note between the ORS and the laser signal from Brno were made to analyse the phase noise. These beating measurements were also used in sections 5.2 and 5.4 to investigate the ORS’ frequency stability.

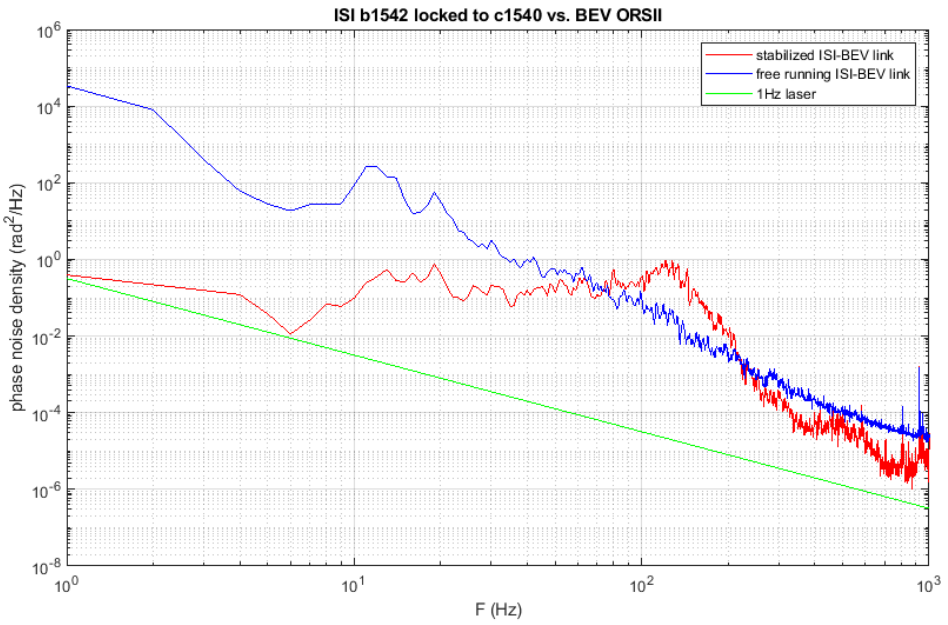

Figure 4.2: Phase noise reduction due to link stabilisation [CPH+21]. The green line represents the profile of a laser with 1 Hz linewidth.

4.2 Fiber link TU Wien

As part of the EMPIR project CC4C a fiber connection from the BEV to the "Atominstitut" (ATI) of the TU Wien was established. This fiber connection makes it possible to trace frequency standards at the ATI to the national frequency standard at BEV. This metrological traceability is realised by transferring the ORS signal to the ATI via a phase-stabilised dark fiber as described in the previous section 4.1. In contrast to the connection between the ISI and the BEV bi-directional amplifiers are not needed, because the distance is a lot shorter. Instead, at the ATI a very stable laser (Koheras Basik by NKT) is phase-locked to the ORS signal from the glass fiber. This offers a relatively cheap opportunity to refresh the stabilised signal from a few µW to 40 mW. The locked Koheras Basik is then frequency doubled with a second harmonic generation (SHG) crystal. The laser light at 771 nm is then used as a traceable reference for experiments at the ATI.

The locking electronics are kindly provided by ISI and implemented in the same chassis that holds the electronics for BEV's side of the ISI-BEV link. For the frequency doubling via second harmonic generation a Magnesium-Doped Periodically Poled Lithium Niobate (MgO:PPLN) crystal is used. The crystal is 40 mm long and has a working temperature of 50 °C or 120 °C depending on which grating on the crystal is used. The yield of the SHG process is strongly dependent on crystal temperature, because the temperature dependency of the refractive index has to be considered for phase matching as discussed in section 2.4. Already half a degree Celsius off the optimal temperature decreases the conversion efficiency noticeably. Consequently, the crystal is kept at a stabilised, steady temperature (±0.01 °C) inside an oven. Another important factor for conversion efficiency is polarisation. Therefore, a half-wave plate is integrated in the setup. The setup is depicted in figure 4.3. The Koheras Basik's light is coupled out of the fiber with a collimator, which determines the light's beam diameter. The beam passes the aforementioned half wave plate, before reaching the first plano-convex lens (L1) for focusing the beam into the center of the PPLN crystal. This process is discussed in section 2.4.1. After the crystal another plano-convex lens (L2) re-collimates the beam and the frequency doubled light is seperated from the fundamental light with a dichroic mirror (M1). The 771 nm light is transferred to the experiments at ATI and the 1542 nm light is used to lock the fibre laser to the ORS.

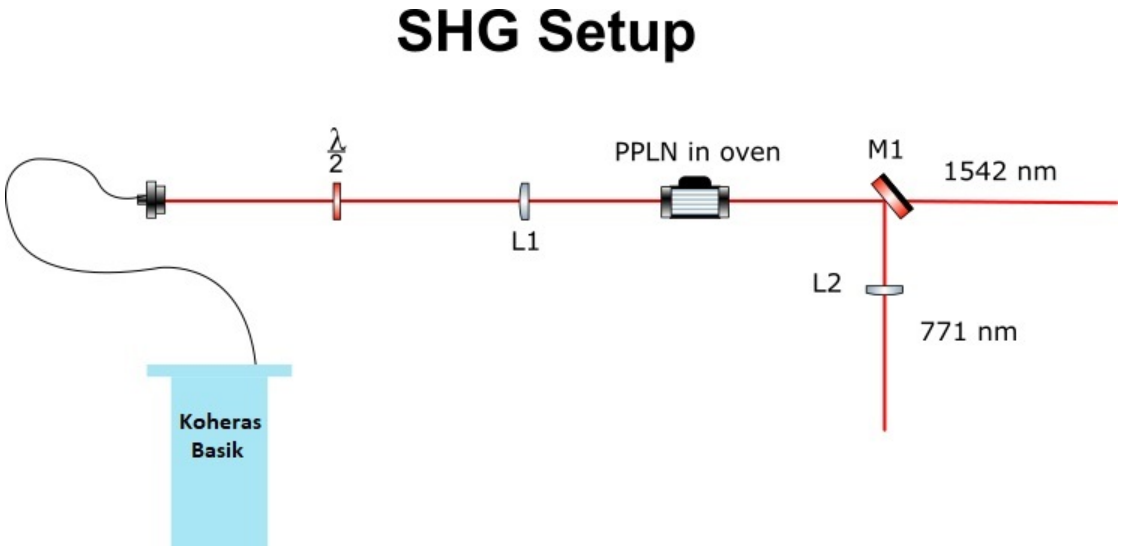

Figure 4.3: Schematic of the second harmonic generation setup.

CHAPTER 5

Characterisation of the Optical Reference System

5.1 Drift Performance

The cavity's drift was measured by a beat-note measurement between a frequency comb and the ORS output. Shortly after delivery, the linear drift was around 150 mHz/s but decreased towards 70 mHz/s over the course of a year. The linear drift has decreased ever since to 20 mHz/s at present, which corresponds to 1.73 kHz/d.

Setup

For the measurement the output of the ORS and the fundamental output of the Ultra low noise (ULN) comb were connected to a "beat detection unit" (BDU) via fibers. The BDU's signal was counted with an FXE frequency counter by K+K Messtechnik [KK]. The raw data provided by the comb's software was processed by a program called "TestComb" [Mic16] by Michael Matus. The program "TestComb" calculates the laser's absolute frequency after the user provides 3 parameters: the signs of the repetition rate and the carrier envelope offset frequency (f_{off}), as well as the mode number of the comb tooth that is closest to the cw laser. The repetition rate and f_{off} are retrieved automatically from the measurement's data file. The visualisation of the processed data was done with the software Origin.

Results

Effectively, the drift data is continuously acquired. So in this section only a selection of data sets is presented as examples to show the cavity's drift performance over time. Figure 5.2 shows four measurements, each over the period of 20000 seconds, which are roughly 5.5 hours. This measurement duration was selected because it is a realistic time

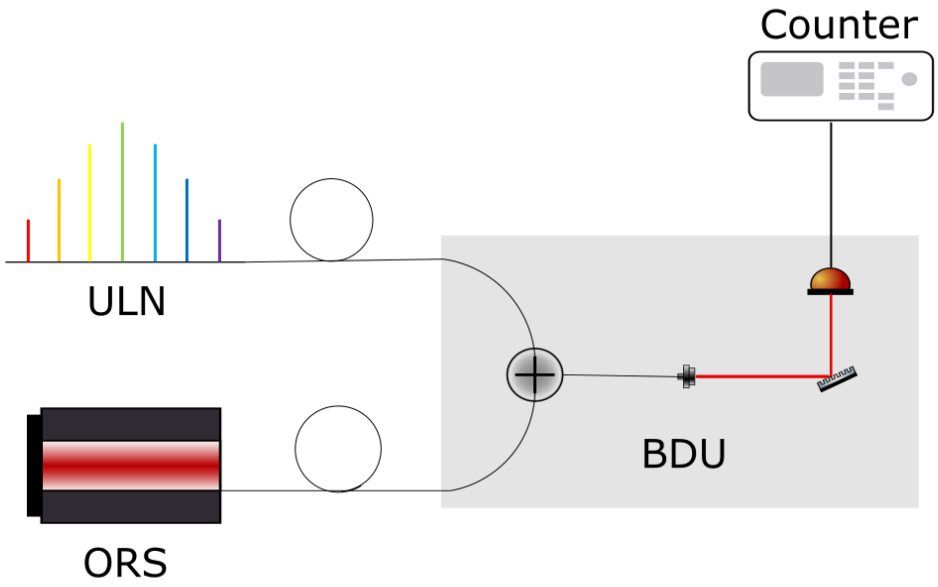

Figure 5.1: Schematic of the beat measurement.[1]

date	linear drift	standard deviation
December 2018	149.53 mHz/s	1.424×10^{-1} mHz/s
June 2019	47.3 mHz/s	1.437×10^{-1} mHz/s
July 2020	14.07 mHz/s	1.312×10^{-1} mHz/s
December 2020	17.34 mHz/s	1.433×10^{-1} mHz/s

Table 5.1: Exemplary results from drift measurements.

frame for real comparison measurements. This is due to the fact that after this period the stability of the free running ORS starts to deteriorate significantly, as can be seen in section 5.2. The results are summarised in table 5.1.

It is worth mentioning that the linear drift is not as well behaved as it appears from these 5.5 hour data sets. As one can see in figure 5.3 there are steps in the ORS's frequency curve. Most of these steps can be directly linked to spikes in the room temperature. This is because the air-conditioning system in the laboratory is not ideal for our application. Some adjustments have already been made and the room temperature stability has improved. However, for reliable measurements the laboratory must not be entered and

[1] The schematic was made in Inkscape using the ComponentLibrary [Ale]

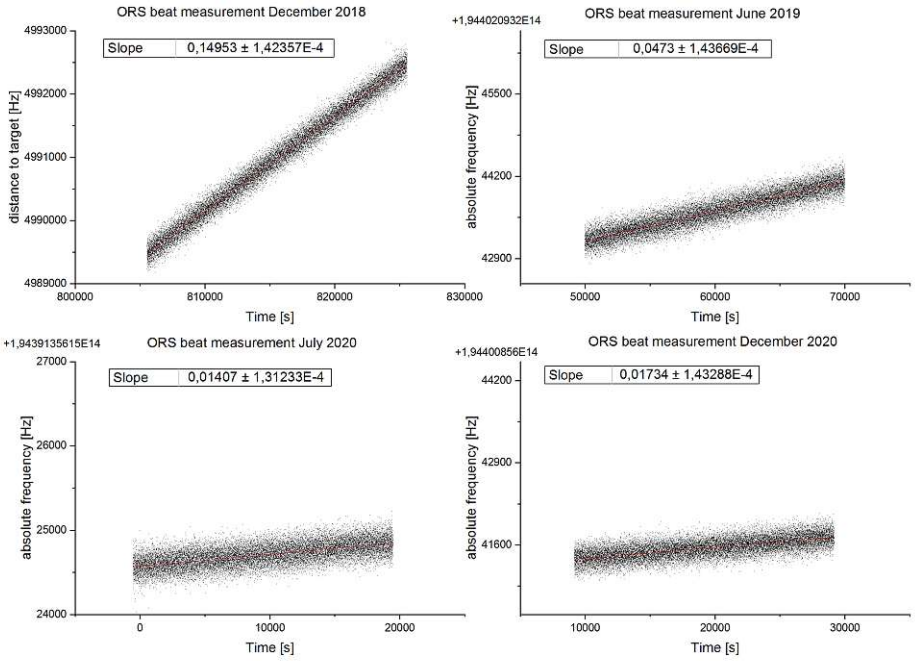

Figure 5.2: Decline of linear drift over time from 150 mHz/s at the time of delivery to below 20 mHz/s at present.

the measurement is controlled remotely. The driving factor for the temperature dependent frequency fluctuations is RAM as discussed in 3.2.1 which introduces an offset to the error signal and shifts the locking point. The laser is then locked to a slightly different frequency.
Also, the linear drift's magnitude changes with temperature around the CTE's zero-crossing temperature [LJW+18]. It is the lowest at the zero-crossing temperature.

It is possible to compensate the ORS' drift by shifting its output with an AOM. The simplest countermeasure would be to change the AOM's RF frequency source at the same rate as the linear drift of the ORS (e.g. 18 mHz/s). This would roughly suppress the overall linear drift, however, as can be seen in figure 5.3, the linear drift rate is not always constant. Moreover, small, non-linear changes to the frequency would not be compensated. There is a more sophisticated way that combines the short-term stability of an ultra-stable laser with the long-term stability of a H-maser. This can be done by optically locking a frequency comb to the ORS. More precisely, with a beating measurement between the ORS and the comb a comb tooth is kept at a constant (frequency) distance to the ultra-stable laser source with a PLL. This locks the repetition rate f_{rep} of the frequency comb generator to the ORS. The carrier envelope offset f_{off}, however, stays locked to the

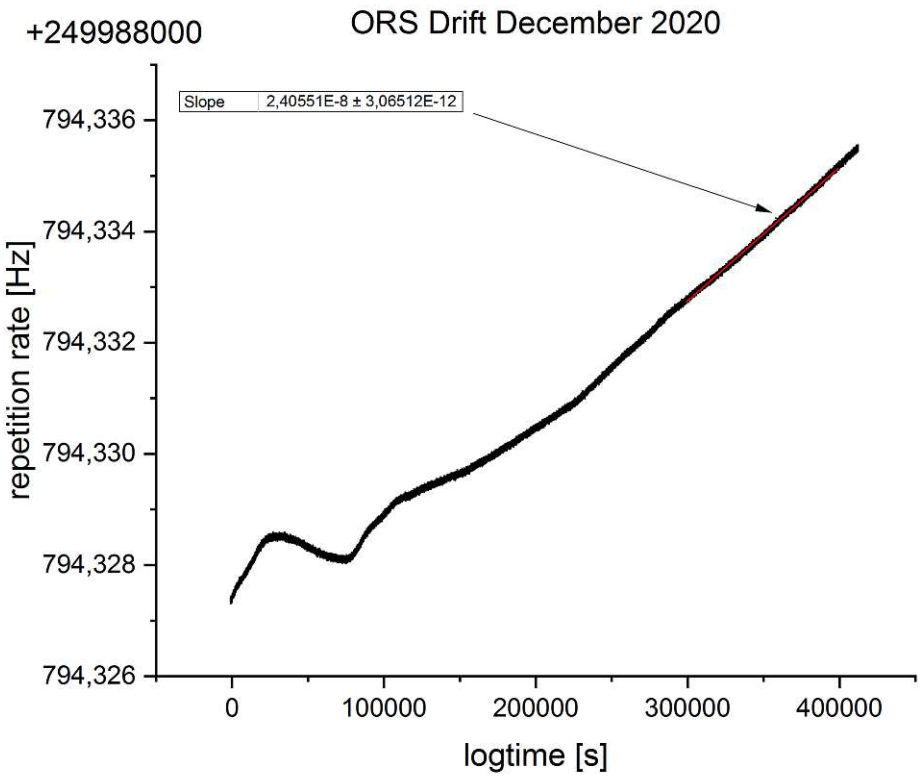

Figure 5.3: Nonlinearities of the ORS's drift. In this case the drift data was collected by measuring the ULN comb's repetition rate which was locked to the ORS. The shown repetition rate drift corresponds to a drift of the ORS of 18.706 mHz/s.

RF reference, which is in this case a maser. Although the maser's stability at 1 second averaging time is roughly two orders of magnitude worse than the laser, there will still be a considerable improvement in the frequency comb's overall short-term stability. Because, when one takes a look at the comb equation

$$f_{\text{Laser}} = m \cdot f_{\text{rep}} \pm f_{\text{off}} \pm f_{\text{beat}} \tag{5.1}$$

one can see that the repetition frequency contributes to the laser frequency with an integer factor m, which is the mode number and of the order of 10^5. So the instability of f_{off} is negligible compared to f_{rep}. A disadvantage of locking the repetition rate to a free running optical reference is that f_{rep} will now drift at the same rate as the laser. To prevent this, one can introduce an AOM into the connection between the ORS and the photodiode that measures the beat. The RF frequency that drives the AOM is varied in such a way that the repetition rate stays at a constant value. This constant frequency value and the AOM driver's frequency are provided by Direct Digital Synthesizers (DDS)

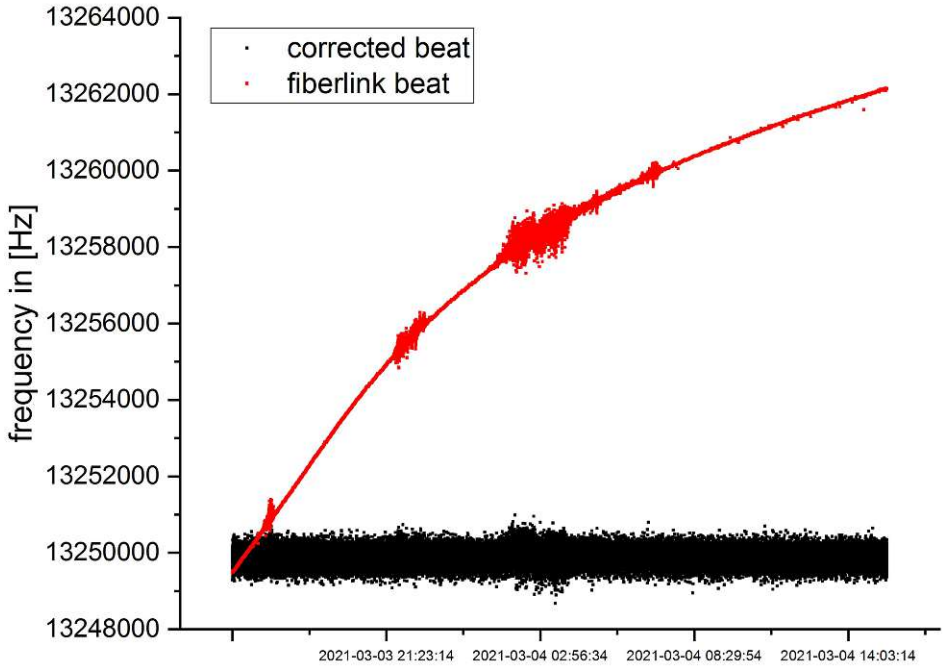

Figure 5.4: In this figure the beat between the ISI's laser and the ORS is shown in red. The black curve is the beat note but corrected for the ORS's drift. This signal is noisier, as the ORS's drift was determined with a comb measurement. This comb measurement, in contrast to the beating measurement, is not processed with a tracking oscillator. One can see that the laser signal from the ISI is not significantly drifting, even though it is locked to a cavity stabilised laser.

that are referenced to the maser. As a consequence, the ORS signal after the AOM will have both the short-term stability of a cavity stabilised laser and the long-term stability of a microwave standard - the best of both worlds. This also means that the output of the compensated ORS no longer shows a drift, linear or non-linear. However, the quality of the compensation depends on how well the control loop is tuned. For example the compensated laser of our colleagues of ISI demonstrates a nicely behaved, constant frequency[2] (see fig 5.4). Such a drift compensation loop is planned for the near future and will greatly improve the ORS' stability performance.

[2]Technically, the laser that was transmitted to and measured at BEV is not the stabilised laser reference. But this transmitted laser is locked to the frequency comb at ISI that is optically locked to their drift compensated reference laser. Hence, a drift in their reference laser would translate into a drift of the transmitted laser.

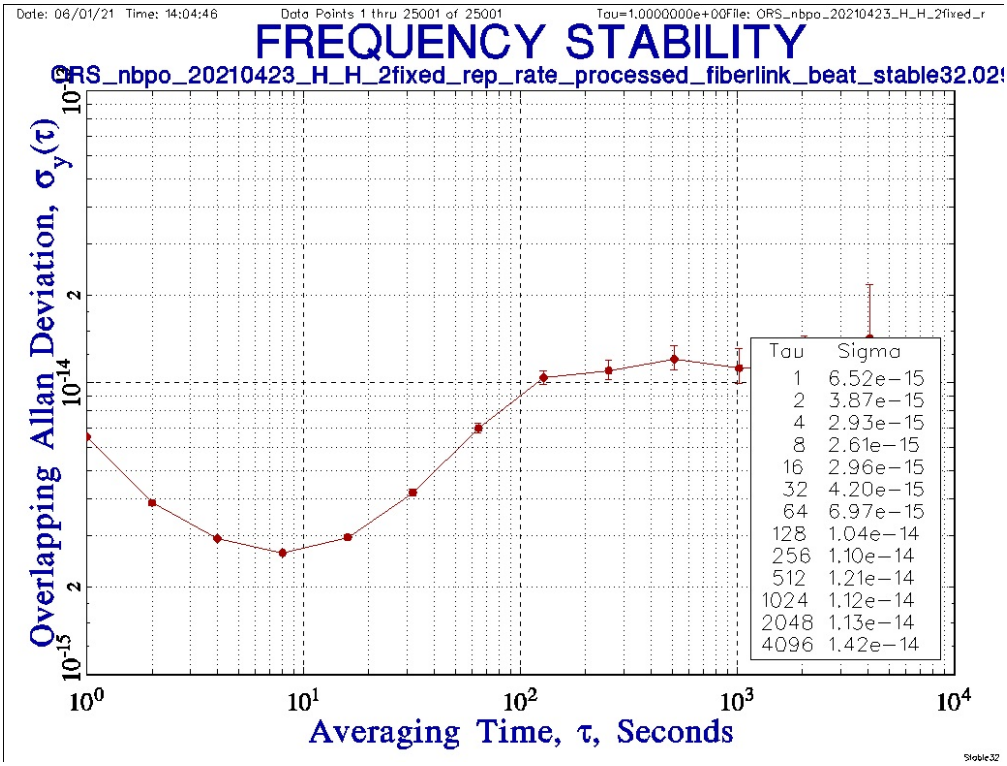

Figure 5.5: ORS fractional frequency stability measured with a beating measurement of two ultra stable lasers.

5.2 Frequency stability

The ORS' frequency stability was measured with a beating measurement and expressed in terms of overlapping allan deviation. The measurements were done with the H-maser referenced frequency comb as the reference oscillator as well as an ultra-stable laser from ISI as the reference oscillator. For the determination of the overlapping allan deviation the ORS's drift was removed via linear regression. Otherwise the linear drift from cavity aging would overshadow the frequency fluctuations from other sources. The drift rates in figures 5.6a and 5.6b differed by about 100 mHz/s, however, after removal of the linear drift the underlying frequency stability is the same in both cases. A comparison with figure 5.5 shows that the frequency stability measured with the frequency comb does not represent the stability of the laser but rather that of the H-maser, especially for averaging times up to 1×10^2 seconds. After this time period the non-linear parts of the drift become noticeable and the laser's stability deteriorates. The measurement shown in figure 5.5 can still be improved, but considering that the two measured lasers are more than 100 km apart, these preliminary results are satisfactory. Improvements in lock performance will move the measured frequency stability closer to the actual frequency stability of the ORS which is in the low 1×10^{-15} range.

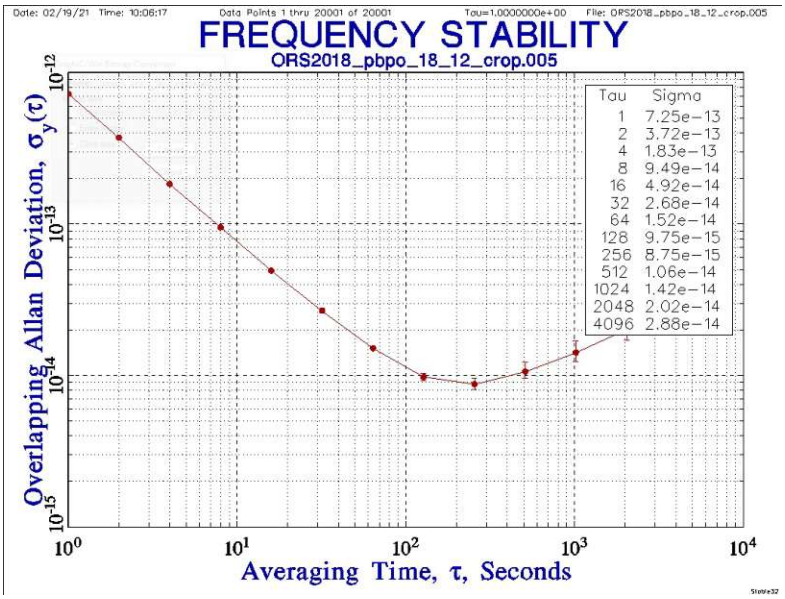

(a)

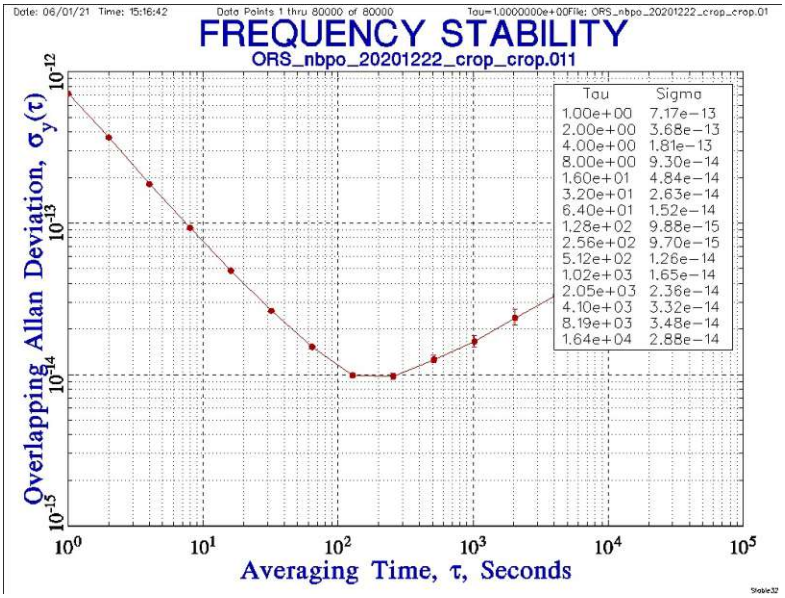

(b)

Figure 5.6: ORS fractional frequency stability measured with a H-maser referenced frequency comb. (a) Measurement taken shortly after delivery in December 2018. (b) Measurement taken in December 2020.

5.3 Zero-crossing Temperature Measurement

The zero-crossing temperature was measured at Menlo Systems and determined to be at a set-temperature[3] of 28.701 °C. To check this setting four measuring points around this preset zero-crossing temperature were taken at 27.701 °C, 28.201 °C, 29.201 °C and 29.701 °C. The measurements took place over the course of three months, from February to May 2021.

Setup

Again, the data was collected with a beating measurement between the ORS and the ULN frequency comb (see fig. 5.1). The starting point of the measurement series was the nominal zero-crossing point of 28.701 °C. The temperature of the cavity was then slowly changed by half a degree to the next measuring point. A slow change of temperature is necessary, so that the lock to the cavity is not lost. After changing the cavity's temperature, the ORS's frequency takes roughly five days to settle and display a steady linear drift of around 20 mHz/s. The frequency change due to thermal expansion of the cavity is in the range of several hundred kHz. Due to the long settling time in-between measurements the data points have to be corrected for linear drift, which is in the range of several kHz per day.

Results

The measured data and the overall shape of the distribution of the data appear to suggest that the zero-crossing temperature of the coefficient of thermal expansion is around 28.2 °C rather than the preset set point of 28.7 °C (see fig. 5.7). This result will have to be checked by another measurement series in the future to verify the determined zero-crossing temperature. At present, however, this is not possible as it requires a time slot of at least three weeks with minimal traffic in the laboratory and no other measurements running.

5.4 Uncertainty Budget

In order to provide an expanded uncertainty for the ORS's frequency, which is traceable to the BEV's frequency standard, an uncertainty budget based on the principles of the "Guide to the expression of uncertainty in measurement" (GUM, [Joi08]) was constructed. In a first step one must define the measurand which is in this case the frequency of the ORS measured with the ULN frequency comb generator. The measurement set-up has three major components that will contribute to the uncertainty budget: the laser itself, the reference frequency and the combined measuring system frequency comb and counter. The estimate for the contributions from the frequency comb, which includes most of the reference frequency's uncertainty contribution, was obtained following the procedure

[3] The displayed value by the built-in sensor will converge to this value.

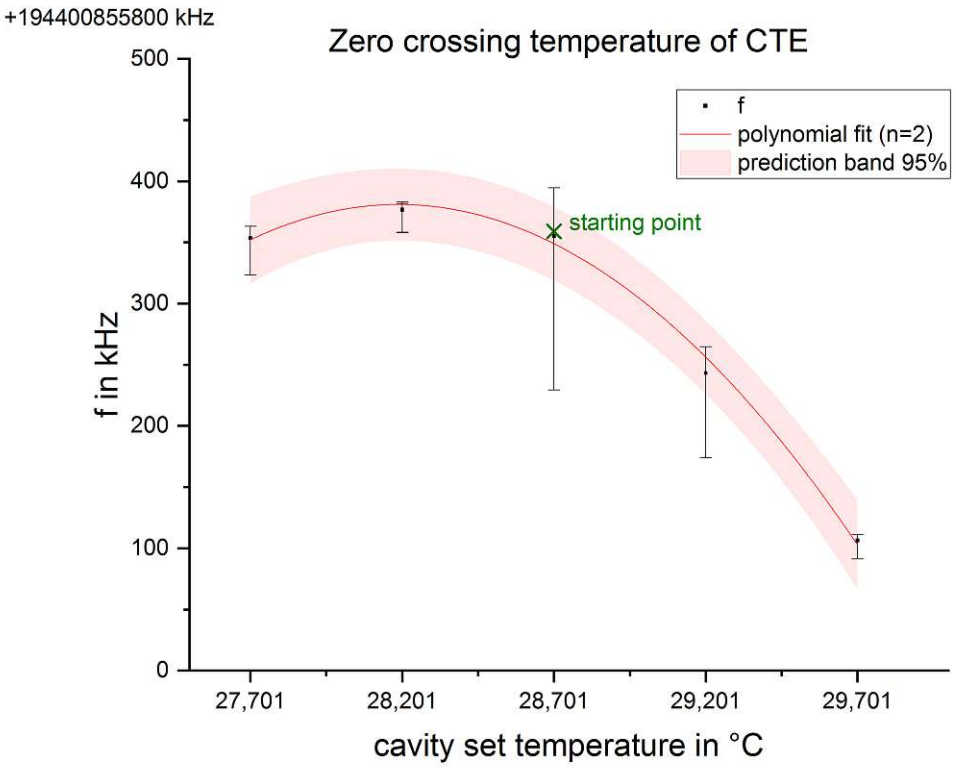

Figure 5.7: Frequency measurements of the ORS at different cavity temperatures. The measurement point titled "starting point" acts as a reference point. All other measurement points were corrected for the frequency drift caused by cavity aging. The mean drift rate was assumed to be 19 mHz/s. For the error bars the maximum drift rate was assumed to be 30 mHz/s and the minimum drift rate was assumed to be 14 mHz/s. The mean drift rate appears to be reasonable, as one can see from the vicinity of the second data point ($\cdot$) at 28.701 °C to the reference point measurement ($\times$), even though it was taken approximately two months after the reference point measurement.

described in the paper [Mat13]. The notation in this section will follow the notation used in the paper. The equation describing the measurand is:

$$f_{\text{Laser}}(t) = n \cdot f_{\text{rep}}(t) + f_{\text{off}}(t) + f_{\text{beat}}(t) + \lambda_r + \lambda_p, \tag{5.2}$$

where f_{rep} and f_{off} are the comb's repetition frequency and carrier envelope offset frequency, f_{beat} is the beat note obtained as described in 5.1. λ_p combines all working parameter specific influences of the laser while λ_r models all other (random) influences. All quantities represent mean values over a given gate time (τ):

$$f(t) = \int_t^{t+\tau} f^{\text{inst}}(t)dt. \tag{5.3}$$

However, in the following notation the explicit reference to t and τ will be dropped. f_{rep} and f_{off} are multiples of a stable input frequency and can be expressed as:

$$f_{\text{rep}} = k_{\text{rep}} f_{\text{in}} + \gamma_{\text{rep}}, \tag{5.4}$$
$$f_{\text{off}} = k_{\text{off}} f_{\text{in}} + \gamma_{\text{off}} \tag{5.5}$$

and

$$f_{\text{in}} = f_0 + \rho. \tag{5.6}$$

Where f_0 is the reference frequency, i.e. the active Hydrogen maser. ρ represents the deviations of the input frequency from the reference frequency, while the γ_i are the deviations of frequency comb related quantities from their ideal value. Finally, the beat note can be separated into a constant value f_b and a small variable part λ_b:

$$f_{\text{beat}} = f_b \frac{f_{\text{in}}}{f_0} + \lambda_b + \gamma_{\text{cnt}} = f_b \left(1 + \frac{\rho}{f_0}\right) + \lambda_b + \gamma_{\text{cnt}}, \tag{5.7}$$

γ_{cnt} accounts for counter specific deviations. After inserting the formulas for the individual quantities in eq. 5.2 one obtains the following expression:

$$f_{\text{Laser}} = f^{\text{N}}_{\text{Laser}} + \frac{f^{\text{N}}_{\text{Laser}}}{f_0}\rho + \gamma + \lambda, \tag{5.8}$$

where $f^{\text{N}}_{\text{Laser}}$ summarizes all the constant quantities that form the nominal frequency of the measured laser. The individual uncertainty contributions γ_i originating from the comb and λ_i originating from the laser were summarized in one quantity, respectively. In (5.8) only ρ, γ and λ are time dependant and, hence, contribute to the uncertainty. The uncertainty of the measurand is the quadratic sum of the input uncertainties

$$u^2(f_{\text{Laser}}) = \frac{(f^{\text{N}}_{\text{Laser}})^2}{f_0^2} u^2(\rho) + u^2(\gamma) + u^2(\lambda) \tag{5.9}$$
$$= u^2(\text{comb}) + u^2(\lambda). \tag{5.10}$$

When traced to the SI second, the uncertainty contribution of the reference frequency ρ has three main origins: the uncertainty of the Cs master clock relative to the international atomic time (TAI) as obtained from circular T, the maximum deviation of H-maser relative to the master clock before steering takes place (dominating influence), and the short-term frequency stability of the H-maser [Mat13] (see fig. 5.8). The H-maser is the limiting factor in terms of uncertainty up to averaging times of 100 seconds. So, in case only the frequency stability is of interest, as it is in section 5.2 the manufacturer's specifications of the H-maser's uncertainty are used, which improves the uncertainty considerably as one can see in fig. 5.10a. The results for the expanded measurement uncertainty with the maser's manufacturer's specifications are given in table 5.5.

The comb's contribution to the uncertainty γ was estimated by comparing the two frequency comb generators that are in service at BEV. For this comparison the ORS was

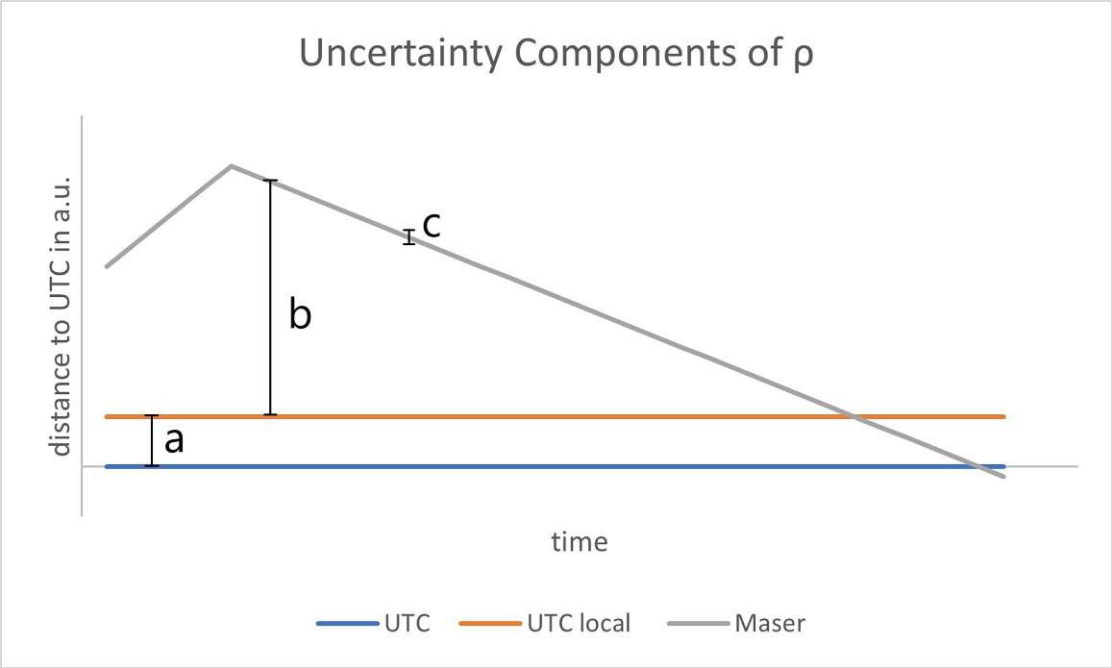

Figure 5.8: Illustration of the three uncertainty contributions associated with the reference frequency f_0. With distance **a** being the uncertainty of the Cs master clock relative to the TAI/UTC[4], **b** being the deviation of the H-maser to the master clock and **c** being the short-term frequency stability of the H-maser.

measured with both combs at the same time with the same counter. By doing this the uncertainty contributions of the reference frequency ρ and of the laser λ drop out, when the two beating measurements are subtracted to obtain Δf_{12}:

$$\Delta f_{12} = f^{\mathrm{N}}_{\mathrm{Laser},1} - f^{\mathrm{N}}_{\mathrm{Laser},2} + \frac{f^{\mathrm{N}}_{\mathrm{Laser},1} - f^{\mathrm{N}}_{Laser,2}}{f_0}\rho + \gamma_1 - \gamma_2 + \delta. \tag{5.11}$$

δ covers setup specific asymmetries (difference in light path, signal delays,...) which are not covered by 5.8. By choosing $f_{b,1}$ and $f_{b,2}$ in such a way that $f^N_{Laser,1} = f^N_{Laser,2}$ one obtains

$$\Delta f_{12} = \gamma_1 - \gamma_2 + \delta \tag{5.12}$$

and

$$u^2(\gamma_1) + u^2(\gamma_2) = u^2(\Delta f_{12}) - u^2(\delta) \tag{5.13}$$

for the uncertainties. One can use the sum of the left-hand side of eq. 5.13 as an upper bound for the uncertainty of the two combs, respectively. Choosing $u^2(\delta)$ to be 0 gives

[4]UTC = TAI + 37s; UTC...coordinated universal time.

the most conservative estimate. For $u(\Delta f_{12})$ one can use the standard deviation from the measurement data for f_{12}. Alternatively, one can use the Allan deviation as it is proportional to the standard deviation of the mean for white phase-noise, which is the case here. For $u(\lambda)$ the contributing factors are imperfections in the PDH locking loop, length changes to the external cavity due to temperature or vacuum pressure and noise collected in the glass fibre connections to the BDU. An estimate for $u(\lambda)$ was acquired by using the standard deviation σ_{Laser} obtained from a beating measurement of the ORS with a laser from ISI that has comparable short-term stability. If there had been three lasers with comparable stability available one could have done a three-cornered-hat comparison, where it is possible to determine the three individual uncertainties [Gra74]. However, since there were only two lasers available, only an upper bound for $u(\text{Laser})$ from the sum of the two standard deviation was determined:

$$u^2(\lambda) = u^2(\text{Laser, ORS}) + u^2(\text{Laser, ISI}) + \text{correlations} = \sigma^2_{\text{Laser}}. \tag{5.14}$$

Since both lasers can be seen as independent, the correlations term is assumed to be zero. Furthermore, it is reasonable to assume that the contribution to $u(\lambda)$ by the ORS is smaller than the one by the ISI laser. This is because $u(\text{Laser, ISI})$ includes uncertainties stemming from the fiber link. For example, the signal from the ISI laser undergoes polarisation rotations along the fiber, because of which the amplitude of the beat signal between the lasers varies. This can cause counting issues and represents a major contribution to the uncertainty. There are also vibrations and temperature gradients along the fiber link that are not compensated by the link stabilisation. Because of the argument above it is justified to at least distribute the uncertainty evenly between $u(\text{Laser, ISI})$ and $u(\text{Laser, ISI})$. Therefore the uncertainty of one laser is

$$u(\text{Laser, ORS}) = \frac{\sigma_{\text{Laser}}}{\sqrt{2}}. \tag{5.15}$$

A similar argument can be made for the comb uncertainties in eq. 5.13 and, hence, the contribution by the comb to the ORS uncertainty is

$$u(\gamma_1) = \frac{u(\Delta f_{12})}{\sqrt{2}}. \tag{5.16}$$

The resulting uncertainty for the ORS as determined in eq. 5.9 is presented in tables 5.2 and 5.3. The expanded measurement uncertainty with a factor of 2 is shown in tables

tau	u(comb)	$u(\lambda)$	u(ORS)
10	15.998 Hz	3.904 Hz	16.467 Hz
100	13.919 Hz	3.752 Hz	14.416 Hz
1000	13.874 Hz	3.244 Hz	14.248 Hz
10000	13.874 Hz	2.832 Hz	14.160 Hz

Table 5.2: Uncertainty results for the ORS.

tau	$u_{\mathrm{rel}}(\mathrm{comb})$	$u_{\mathrm{rel}}(\lambda)$	$u_{\mathrm{rel}}(\mathrm{ORS})$
10	8.230×10^{-14}	2.008×10^{-14}	8.471×10^{-14}
100	7.160×10^{-14}	1.930×10^{-14}	7.416×10^{-14}
1000	7.137×10^{-14}	1.669×10^{-14}	7.329×10^{-14}
10000	7.137×10^{-14}	1.457×10^{-14}	7.284×10^{-14}

Table 5.3: Relative uncertainty results for the ORS.

tau	$U^{\mathrm{traced}}(\mathrm{ORS})$	$U_{\mathrm{rel}}^{\mathrm{traced}}(\mathrm{ORS})$
10	32.934 Hz	1.694×10^{-13}
100	28.832 Hz	1.483×10^{-13}
1000	28.496 Hz	1.466×10^{-13}
10000	28.320 Hz	1.457×10^{-13}

Table 5.4: Expanded uncertainty results for the ORS traced to the SI second.

tau	$U^{\mathrm{specification}}(\mathrm{ORS})$	$U_{\mathrm{rel}}^{\mathrm{specification}}(\mathrm{ORS})$
10	17.730 Hz	9.120×10^{-14}
100	7.845 Hz	4.035×10^{-14}
1000	6.597 Hz	3.393×10^{-14}
10000	5.754 Hz	2.960×10^{-14}

Table 5.5: Expanded uncertainty results for the ORS.

5.4 and 5.5.

Generally, it can be seen that the reference frequency poses a limiting factor for the traceable uncertainty. If one takes the H-maser's specifications as a base for the uncertainty, the current knowledge about the laser's uncertainty poses the limiting factor. This knowledge, however, will improve in the near future, due to improvements of the link stability BEV-ISI.

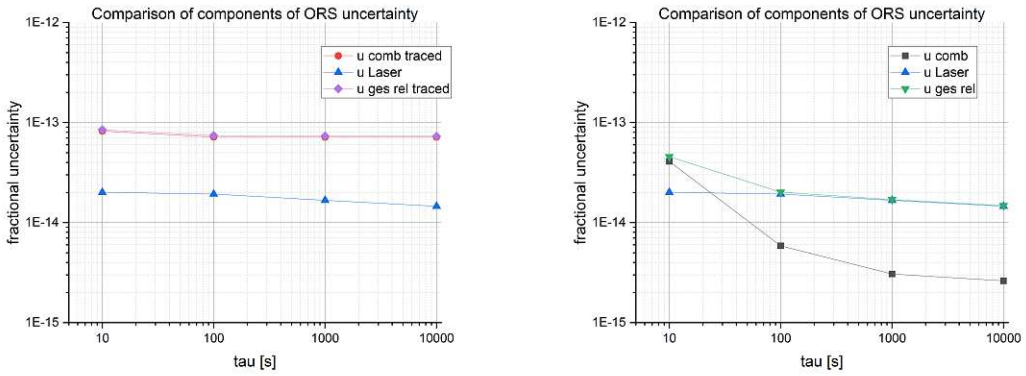

(a) (b)

Figure 5.9: Comparison of components that contribute to the ORS uncertainty. In case of the uncertainty traced to TAI the reference frequency in the comb budget is the limiting factor for the ORS uncertainty (a). If the manufacturer's specifications are used for the reference frequency, the knowledge about the laser's contribution to the ORS uncertainty budget is the limiting factor (b).

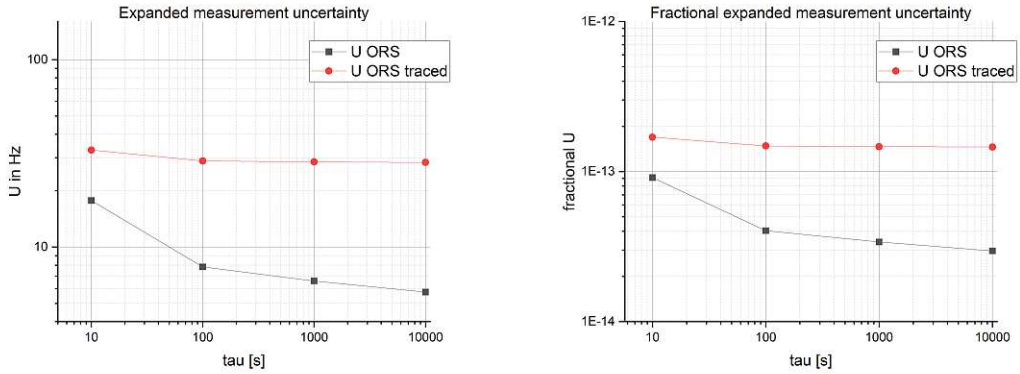

(a) (b)

Figure 5.10: Expanded measurement uncertainty as an absolute number in Hz in (a) and U_{rel} in (b).

CHAPTER 6

Conclusion & Outlook

In the course of this thesis, the optical reference system of the BEV was characterised. The characterisation included measurements of the frequency stability, cavity drift and zero-crossing temperature, as well as a calculation of an uncertainty budget of the emitted frequency traceable to UTC.

The fractional frequency stability was found to be of the order of 10^{-15}. Depending on the used comparison oscillator the lowest instability was reached for averaging times of 10 s for the laser-laser comparison, respectively, 200 s for the maser-laser comparison. The stability measurement in terms of laser-laser comparisons can still be improved by comparing the ORS to a more stable reference laser, or by improving the stability of the fiber link to the laser that is currently used. The maser-laser comparison cannot be easily improved in the short term region due to limitations of the microwave reference. In the long term region of averaging times of more than 100 s some improvements in the measured instability could be made by compensating for the cavity's drift.

The linear cavity drift due to cavity aging was determined to be below 20 mHz/s. There are, however, occasional prominent non-linearities in the ORS' frequencies drift, which are mostly not related to the cavity, but rather to residual amplitude modulation caused by the EOM used in the PDH locking scheme. To reduce the influence of RAM the temperature around the optical setup of the ORS should be kept as constant as possible. One improvement could be a chamber around the ORS that decouples it from the rest of the room and reduces convection and drafts around the laser.

The measured value of the cavity's zero-crossing temperature was 28.201 °C. This measurement should be repeated in the future to confirm the result. This kind of measurement, however, is quite tedious, due to the long settling time ($\approx$ 5 days) of the frequency drift to show a linear behaviour again, after changing the cavity temperature.

The expanded measurement uncertainty traced to UTC was determined as 1.7×10^{-13} to 1.5×10^{-13}, respectively, 32.93 Hz to 28.32 Hz depending on the averaging time. The limiting factor for the uncertainty budget with the current setup, in the case where it is

traced to UTC, is the microwave reference oscillator. A more sophisticated uncertainty estimate for the reference frequency can improve the traced uncertainty one can give for a comb measurement. Furthermore, the contribution to the uncertainty budget by the laser can be reduced by a more rigorous classification and quantification of uncertainty sources.

List of Figures

List of Tables

Bibliography

[Ale] Alexander Franzen. ComponentLibrary. http://www.gwoptics.org/ComponentLibrary/. Accessed: 2021-01-14.

[BK68] G. Boyd and D. Kleinman. Parametric interaction of focused gaussian light beams. *Journal of Applied Physics*, 39(8), 1968.

[Bla00] Black, Eric D. An introduction to Pound–Drever–Hall laser frequency stabilization. *American Association of Physics Teachers*, April 2000.

[Cip19] Ondrej Cip. Brno Vienna infrastructure scheme, 2019.

[Cor] Corning Incorporated. ULE® Corning Code 7972 - Ultra Low Expansion Glass. https://www.corning.com/media/worldwide/csm/documents/D20FD2EA-7264-43DD-B544-E1CA042B486A.pdf. Accessed: 2020-12-22.

[Cov] Covesion Ltd. How to Use PPLN. https://www.covesion.com/resource/how-to-use-ppln/. Accessed: 2021-06-09.

[CPH+21] Martin Cizek, Lenka Pravdova, Jan Hrabina, J Lazar, Thomas Pronebner, Jörg Premper, Elke Aeikens, O Havlis, V Smotlacha, L Altmannova, Thorsten Schumm, J Vojtech, Anton Nießner, and Ondrej Cip. Fibre link for optical frequency transfer between ISI and BEV. *submitted to IEEE Xplore*, 2021.

[Edm] Edmund Optics Ltd. UK. Gaussian Beam Propagation. https://www.edmundoptics.eu/knowledge-center/application-notes/lasers/gaussian-beam-propagation/. Accessed: 2021-06-09.

[fTF16] Consultative Committee for Time and Frequency. CCTF strategy document. https://www.bipm.org/utils/en/pdf/CCTF-strategy-document.pdf, May 2016. Accessed: 2021-02-09.

[GBK+21] Patrick Gill, Geoffrey Barwood, H.A. Klein, H.s Margolis, Stephen Webster, Fritz Riehle, Ekkehard Peik, Harald Schnatz, Uwe Sterr, Gerhard Hejc, Alexander Pawlitzki, and Diana Portolés. Feasibility and applications of optical clocks as frequency and time references in esa deep space stations. 07 2021.

[Gen18] General Conference on Weights and Measures (CGPM). *26th meeting of the CGPM – Proceedings*, 2018.

[Gra74] Gray, J and Allan, D. A method for estimating the frequency stability of an individual oscillator. *Proceedings of the 28th Annual Symposium on Frequency Control*, pages 243–246, 1974.

[ITU20] Spectral grids for WDM applications: DWDM frequency grid, October 2020. http://handle.itu.int/11.1002/1000/11482.

[Joi08] Joint Committee for Guides in Metrology (JCGM/WG 1). Evaluation of measurement data — Guide to the expression of uncertainty in measurement. https://www.bipm.org/en/publications/guides/gum.html, September 2008. Accessed: 2021-01-18.

[KK] K+K Messtechnik. http://kplusk-messtechnik.de/products/fxe_19.htm#top. Accessed: 2021-07-11.

[LJW+18] Hui Liu, Kun-Liang Jiang, Jin-Qi Wang, Zhuan-Xian Xiong, He Ling-Xiang, and Bao-Long Lu. Precise calibration of zero-crossing temperature and drift of an ultralow expansion cavity with a clock transition spectrum. *Chinese Physics B*, 27(5), 2018.

[Lut17] Lutus, Paul. OpticalRayTracer 8.9. https://arachnoid.com/OpticalRayTracer/, 2017. Accessed: 2021-06-10.

[Mat13] Matus, Michael and Balling, Petr and Mache, Werner and Nießner, Anton and Kren, Petr. Uncertainty estimation for comb based laser calibrations by direct comparison of 3 different combs. August 2013.

[Mena] Ultrastable lasers. https://www.menlosystems.com/products/ultrastable-lasers/ors/. Accessed: 2021-07-11.

[Menb] Menlo Systems. ORS cavity 3w. https://www.menlosystems.com/products/ultrastable-lasers/ors-cavity/. Accessed: 2020-12-21.

[Men18] Menlo Systems. *User Manual - ORS1500 Optical Reference System*, 2018.

[Mic16] Michael Matus. TestComb version 0.992.7193.21554, 2016.

[MJYH94] Long-Sheng Ma, Peter Jungner, Jun Ye, and John Hall. Delivering the same optical frequency at two places: accurate cancellation of phase noise introduced by an optical fiber or other time-varying paths. *Optics Letters*, 19(21), November 1994.

[MS21] B. L. S. Marlow and D. R. Scherer. A review of commercial and emerging atomic frequency standards. *IEEE Transactions on Ultrasonics, Ferroelectrics, and Frequency Control*, 2021.

[Rie06] Fritz Riehle. *Frequency Standards: Basics and Applications*. John Wiley Sons, 2006.

[Sha08] Shaoul, Ezekiel. RES.6-005 Understanding Lasers and Fiberoptics. https://ocw.mit.edu/resources/res-6-005-understanding-lasers-and-fiberoptics-spring-2008/index.htm#, 2008. Accessed: 2021-05-11.

[Sul15] Suliman, Tamir. Fabry Perot filter modeling and Analysis. https://de.mathworks.com/matlabcentral/fileexchange/39625-fabry-perot-filter-modeling-and-analysis, 2015. Accessed: 2021-05-16.

[UHH02] Thomas Udem, Rondald Holzwarth, and Theodor Hänsch. Optical frequency metrology. *Nature*, 2002.

[Wik08] Wikimedia Commons. Laguerre-gaussian.png. https://commons.wikimedia.org/wiki/File:Laguerre-gaussian.png, 2008. Accessed: 2021-05-18.

[ZMB+14] W. Zhang, M. J. Martin, C. Benko, J. L. Hall, J. Ye, C. Hagemann, T. Legero, U. Sterr, F. Riehle, G. D. Cole, and M. Aspelmeyer. Reduction of residual amplitude modulation to 1×10^{-6} for frequency modulation and laser stabilization. *Opt. Lett.*, 39(7):1980–1983, Apr 2014.